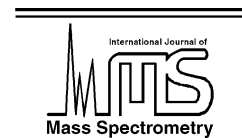




ELSEVIER

International Journal of Mass Spectrometry 220 (2002) 419–441



www.elsevier.com/locate/ijms

Gas-phase reactions of bare and oxo-ligated actinide and lanthanide cations with pentamethylcyclopentadiene studied in a quadrupole ion trap mass spectrometer

Glen P. Jackson, John K. Gibson*, Douglas C. Duckworth

Chemical Sciences Division, Oak Ridge National Laboratory, P.O. Box 2008, Oak Ridge, TN 37831-6375, USA

Received 3 June 2002; accepted 22 July 2002

Abstract

Reactions of bare and oxo-ligated monovalent ions of uranium and thorium with 1,2,3,4,5-pentamethylcyclopentadiene, $C_{10}H_{16}$, (HCp^*) were examined in a quadrupole ion trap (QIT) mass spectrometer. Representative lanthanide ions, Ln^+ and LnO^+ , and tantalum ions, Ta^+ and TaO^+ , were studied for comparison. The product branching ratios for both primary and secondary reactions of the actinide ions demonstrated gas-phase organoactinide chemistry that is quite disparate from organolanthanide chemistry under comparable conditions for this neutral reactant. Particularly revealing were product distributions for ThO^+ and UO^+ , which indicated chemical behavior similar to that of bare Sm^+ . We conclude that at least one valence electron at the metal center of the actinide oxide ions must remain chemically active. In the case of UO^+ , this provides evidence for the chemical engagement of the quasi-valence 5f electrons, which is in distinct contrast to the inert character of the 4f electrons of the lanthanides in both Ln^+ and LnO^+ . Mass-selective chemistry of two primary products, $UC_{10}H_{10}^+$ and $UC_9H_8^+$, also showed behavior similar to that of Sm^+ and UO^+ , implying that there are two covalent organouranium bonds in these complex ions. In comparing the QIT results for the lanthanides with those from a low-pressure ion cyclotron resonance (ICR) mass spectrometry study [Organometallics 16 (1997) 3845], qualitative agreement was found, but significant quantitative differences were apparent. Based on results from collision-induced dissociation and effects of variations in bath gas pressure in the QIT, we conclude that the discrepancies arise from the very different pressure regimes in the ICR and QIT. Evidently, the QIT can be operated over a range of pressures that manifest effects of collisional cooling for some reactions. For the lowest pressure QIT experiments, the high degree of fragmentation is reminiscent of the ICR results. We propose that the QIT bath gas can essentially act as an inert “solvent,” which serves to mediate high-energy processes due to energy transfer from nascent hot intermediate products via energy-dissipating collisions. (Int J Mass Spectrom 220 (2002) 419–441) © 2002 Elsevier Science B.V. All rights reserved.

Keywords: Gas-phase metal ion–molecule chemistry; Actinide; Bath gas effect; Quadrupole ion trap; Lanthanide

1. Introduction

Many aspects of the gas-phase organometallic chemistry of several transition metal ions, M^+ , have been investigated using ion cyclotron resonance (ICR)

mass spectrometry [1,2]. Aspects of organometallic chemistry of ions of the 4f-block lanthanides (Ln) [3–11], as well as of the two predominant naturally occurring 5f-block actinides, Th [12,13] and U [13–15], have also been studied by ICR. The two common types of ion traps are the Penning trap, which is used in ICR, and the Paul trap, which is the

* Corresponding author. E-mail: gibsonjk@ornl.gov

basis for the quadrupole ion trap (QIT) mass spectrometer. The characteristics of these two types of trapped ion mass spectrometers have been described and compared in the context of their applications in elemental analysis [16]. Although ICR has been the dominant technique in recent years for investigating gas-phase metal ion chemistry, QIT has been employed to investigate other aspects of gas-phase ion chemistry. Among the first reactions studied in a QIT were proton transfers between organics [17]; recent work has included complexation of transition metal ions by crown ethers [18]. Several studies in recent years have examined organic ion–molecule reactions in QITs [19], but studies of metal ion–molecule chemistry by this technique remain largely neglected.

The primary goals of the present study were to elucidate the gas-phase ion chemistry of actinide elements, and to evaluate QIT as a technique for probing gas-phase organometallic ion chemistry, particularly in comparison with ICR. The chemistry of bare and oxo-ligated Th and U ions were examined and compared with the chemistry of the corresponding ions of representative lanthanides, Ln = La, Pr, Nd, Sm and Gd, and the 5d-block transition metal, Ta; all ions were studied under similar conditions in the QIT. The 1,2,3,4,5-pentamethylcyclopentadiene (HCp*) reaction substrate was selected because lanthanide ion chemistry with HCp* has been studied by ICR [20,21], allowing direct comparison of results obtained by the two trapped ion mass spectrometry techniques. The lanthanide results from the previous ICR experiments revealed two distinctive types of reactivity that reflected the electronic structure and energetics at the metal ion center.

Previous results for reactions of bare and oxo-ligated uranium ions with HCp* studied by a time-of-flight approach [22] suggested distinctive behavior which may illuminate the role of the actinide 5f electrons in organometallic chemistry. It was desirable to perform mass-selected chemistry in an ion trap to definitively discriminate between the chemistries of U^+ , UO^+ and UO_2^+ , and obtain more quantitative results to better address the discrepancies between the actinides and lanthanides, in the particular context of the role

of electronic structures and energetics which are distinctive to the 5f actinide series of elements. Some secondary reaction pathways of particular interest were examined by QIT via mass-selective isolation of primary products. Because of the exceptionally high reactivity of the HCp* substrate, comparisons between absolute reaction efficiencies are not particularly enlightening. Rather, it is the distinctive fragmentation pathways that have provided insights into the role of electronic structures and energetics [21]. Significant discrepancies were observed in the reaction branching ratios for lanthanide ion chemistry between the earlier ICR results and those obtained in a QIT in the present work. The origins of these differences were probed by varying experimental conditions in the QIT. Parameters of particular interest were the bath gas pressure (variable “cooling”), and resonant excitation (variable “heating”) of product ions. The dependence of the product ion distributions on the bath-gas pressure is especially intriguing. The observations are interpreted in the context of the role of collisional cooling and stabilization of nascent “hot” intermediates that may undergo further fragmentation under low-pressure conditions, as are encountered in ICR.

2. Experimental

The fundamental aspects of the theory, design and operation of the QIT, including those involving the pulsed glow discharge ion source, have been described in detail elsewhere [16]. The following naturally occurring or highly enriched isotopes were used in the glow discharge ion source: La-139, Pr-141, Nd-142, Sm-144, Gd-160, Ta-181, Th-232 and U-238. For La, Gd, Ta, and U, natural abundance metal samples were placed directly in the sample holder of a direct insertion probe [23,24]. The insertion probe was mounted in a six-way cross that was fitted to the front end of a QIT, as described earlier [25]. For the Pr and Sm studies, oxide samples (Ln_2O_3) were pressed onto a gold pin-cathode for sputtering. Hydrated thorium formate, $Th(HCO_2)_4 \cdot 4H_2O$, was also pressed onto a gold pin for sputtering, and bare and oxo-ligated thorium ions

could be extracted from the glow discharge source without complication.

A combination of techniques familiar to QIT users was used to isolate specific isotopes of metal ions before cooling and reacting them with HCp*. These included (i) adjusting the trapping potential in order to limit the low-mass cut off of ions that are stable in the trap, and (ii) by using filtered noise fields (FNFs) [26]. FNFs are supplementary waveforms that are applied to the end cap electrodes of the QIT in order to eject ions that are not desired. Following isolation, the metal ions were allowed to collisionally cool at a low trapping potential ($q_z \approx 0.3$) while several additional frequencies continually ejected any reaction products that formed during this time. After 20–30 ms of cooling, the ejection frequencies were removed and the products from reactions of the cooled ions were trapped and monitored as a function of reaction time.

For experiments involving oxo-ligated ions, the above approach was used but with the addition of 1×10^{-6} Torr O₂ to the trap (corrected pressure, see below for details). Additional time (~50 ms) after the ion accumulation period allowed the bare metal ions to form their oxo-ligated counterparts. After sufficient populations of oxide ions were formed, FNF frequencies were used to isolate the metal oxide ion of interest before applying the cooling and reaction periods as described above.

To study sequential reactions, the products of the initial reactions of metal ions with HCp* were subjected to the equivalent of a notch filter in the FNF frequencies to isolate a specific primary product. The isolated product was then allowed to further react for a designated time period (typically ~10 ms) before the final mass spectrum was collected. In select cases, attempts to isolate weakly-bound products resulted in the dissociation/fragmentation of the product due to off-resonance excitation. That is, the ions being isolated were accelerated by frequencies that were close to the fundamental secular frequency of their motion, causing them to dissociate as a result of relatively low-energy collisions with the bath gas. Currently, there is insufficient knowledge to determine absolute bond energies or binding constants from such

off-resonance excitation, although much work has focused on quantifying on-resonance excitation [27–29].

Collision-induced dissociation of certain products was achieved after the isolation of a specific initial product of the reactions of metal ions with HCp*. For this, isolated ions were subjected to an on-resonance excitation voltage applied in a dipolar fashion to the end caps of the ion trap [30]. It is possible to apply increasingly larger excitation amplitudes using an automated program in order to qualitatively assess the heating effect on the degree and type of fragmentation/dissociation as a result of relatively high-energy collisions with the neon bath gas.

Gas pressures were measured using an ion gauge mounted on the side of the vacuum chamber that contained the trap. Based on the factory calibration and the configuration of the gas-inlet and pumping system, the measured pressures, after correction for gauge sensitivity, should reasonably accurately represent the pressures in the ion trap. The HCp* pressure was held constant at $\sim 5 \times 10^{-6}$ Torr, uncorrected for ion gauge sensitivity. Assuming an ion gauge sensitivity of ~10 for HCp* [31,32], the actual HCp* pressure is estimated as $\sim 5 \times 10^{-7}$ Torr. This is comparable to the pressures employed in the previous ICR experiments with HCp*, and three-body reactions involving two HCp* molecules can be excluded [21]. The Ne bath gas pressure was generally maintained at $\sim 4 \times 10^{-4}$ Torr, corrected for the gauge sensitivity for Ne of 0.3 [31]. For some specified experiments, the bath gas pressure was varied to ascertain effects of this parameter on product distributions.

3. Results and discussion

All of the tabulated ion–HCp* reaction product distributions were obtained from composite mass spectra which were acquired by averaging several discrete mass spectra, each corresponding to a reaction period of ~10 ms. The product distributions for shorter and longer reaction periods were essentially the same. The consistency of the primary product branching ratios over a range of reaction times indicates that the

primary reactions correspond to interaction of a metal or oxide ion with a single HCp* molecule. Results were obtained for primary reactions of an ion with a single HCp* molecule, as well as secondary reactions of primary product ions with a second HCp*.

Previous ICR studies for reactions of lanthanide ions with HCp* [21] revealed high reaction efficiencies for all of the bare and oxo-ligated lanthanide ions with HCp*. The reaction rate efficiencies, k/k_{ADO} , derived from the ICR studies were between 0.3 (Yb⁺) and 0.8 (La⁺) for the bare lanthanide ions, and between 0.5 (NdO⁺) and 0.9 (YbO⁺) for the oxo-ligated lanthanide ions. Because all of the primary reaction rates in the present study were comparable for all studied M⁺ and MO⁺ to within a factor of ~3, no attempt was made to measure absolute reaction rates in the QIT, although this can be accomplished in a straightforward manner. Based on the previous ICR results [21] and the similar rates observed for all of the ions studied in the present work, it is confidently concluded that all of the studied ions react rather efficiently with HCp*: i.e. $k/k_{\text{ADO}} > 0.1$. The high reactivity of an ion such as Sm⁺, which is relatively inert towards most cyclic alkenes, is attributed to the distinctive properties of the HCp* substrate, which is highly susceptible to attack and subsequent fragmentation [21]. The total number of product ions in the trap after the 10 ms reaction period was typically a few percent relative to the remaining unreacted M⁺ or MO⁺, indicating a low probability for ion–HCp* collisions under these conditions. This was confirmed by the absence of significant amounts of secondary reaction products for short reaction times (<10 ms).

The results for the product distributions for the primary and secondary reactions of M⁺, MO⁺ and UO₂⁺ are presented. The secondary reaction product distributions correspond to reactions of the primary products with a second HCp* molecule. Tertiary products were sought for U⁺, UO⁺ and UO₂⁺ and none were found. The low probability for a third HCp* molecule to associate to secondary products can be attributed to the bulky nature of the HCp* ligand. In view of the particular interest in the nature of the bonding in organouranium complexes, experiments were carried

out in which the most abundant primary products from the {U⁺ + HCp*} reaction were isolated prior to subsequent secondary reactions. The lanthanide results are compared with those from ICR. Of special interest is the particular behavior of the actinides, thorium and uranium, as their chemistry can illuminate the role of the quasi-valence 5f electrons on actinide reactivity in the gas phase. Tantalum was included as representative of a highly reactive d-block transition metal ion. The results for primary and secondary reactions of M⁺ and MO⁺ with HCp* are summarized in the tables as product distributions; the ICR results from Marçalo et al. [21] are included for comparison.

3.1. Reactions of M⁺ with HCp*

3.1.1. Primary products

The product distributions for reactions of the bare metal ions, M⁺, with HCp* are given in Table 1. The results are presented as the relative product ion abundances (peak heights) of product ions with a net composition, M[HCp* – E]⁺; HCp* is C₁₀H₁₆, and the aggregate of eliminated atoms, E, are expressed as likely neutral species. For example, net loss of CH₅ is expressed as {H₂,CH₃}, with the caveat that we have no direct evidence for specific formulations. In this particular case, the alternative assignment of {CH₄,H} is considered less probable, based on the discussed chemistry. In most cases, the specified molecular formulations such as {H₂,CH₄} are confidently considered valid; the uncertainty is greater where one of the eliminated species must be a radical rather than a stable molecule. For the five studied bare lanthanide ions, it is evident that there is reasonable qualitative agreement between the QIT and ICR results [21]. Discrepancies between the product abundance distributions for the two techniques are addressed below. Specifically, effects of bath gas pressure on product distributions are interpreted in the context of the significant quantitative differences between the ICR and QIT results.

The reactivity of the Ln⁺ was discussed by Marçalo et al. [21] in the context of the energy needed to excite the ground state metal ions to a configuration with two chemically active non-f valence electrons.

Table 1
Primary product distributions from reactions of bare metal ions with HCP*^a

<i>E</i> ^b	La ⁺	Pr ⁺	Nd ⁺	Sm ⁺ ^c	Gd ⁺	Th ⁺	U ⁺	Ta ⁺ ^d
H	–	–	–	–	6	5	–	–
CH ₃	–	–	–	–	48	40	–	–
H ₂	32	<i>12</i>	47	<i>36</i>	50	38	37	55
2H ₂	9	<i>27</i>	–	<i>15</i>	–	10	–	13
3H ₂	8	<i>17</i>	–	<i>4</i>	–	6	–	8
CH ₄	27	<i>12</i>	48	<i>32</i>	50	27	–	31
H ₂ ,CH ₄	4	<i>11</i>	–	<i>4</i>	–	7	–	7
2H ₂ ,CH ₄	4	<i>5</i>	–	–	–	–	–	5
C ₂ H ₆	–	<i>7</i>	–	<i>9</i>	–	–	–	6
H ₂ ,H	–	–	–	–	–	–	–	–
H ₂ ,CH ₃	–	–	–	–	–	–	–	–
							13	
							25	

^a The values are percentages of the total primary product yield. Products at ≤2% yield are not included. The variation between experiments for minor products (<10%) was within a factor of 2. The cited values for the major products (≥10%) were reproducible to within ±5. For each of the lanthanides, the italicized values are the ICR result from Marçalo et al. [21]. Non-observed products are designated by a “–”. Minor (<5%) *E* = {H₂, C₂H₆} and {2H₂, C₂H₆} products for La⁺ and Gd⁺ have been excluded for lucidity.

^b The products are {MC₁₀H₁₆ – *E*}⁺, where the eliminated moieties, *E*, are given.

^c A QIT-MS product unique to Sm⁺ was 5% {SmC₁₀H₁₆–CH₂}⁺.

^d Several additional products were evident only for Ta⁺: elimination of {2H₂,H} (3%); {3H₂,H} (3%); {4H₂} (24%); {4H₂,H} (3%); {5H₂} (5%); {3H₂,CH₄} (3%); {3H₂,C₂H₆} (5%); and {H₂,C₄H₁₀} (3%).

For the metal ions studied in the present work these promotion energies, as well as the ground and excited state electronic configurations, are included in Table 2. These energies correspond to a 4f → 5d excitation for the Ln⁺, and to a 7s → 6d excitation for U⁺; no excitation is needed in the case of Th⁺. The efficient activation of HCP* by Ln⁺ results in two distinctive fragmentation patterns: (1) non-insertion type, as illustrated by the results for Sm⁺ in Table 1; and (2) insertion type, as illustrated by the results for the other four Ln⁺ in Table 1. Non-insertion type fragmentation corresponds primarily to H-, CH₃- and H₂-loss, and is exhibited by those Ln⁺ with the largest promotion energies. For Sm⁺, Eu⁺ and Yb⁺, H-, CH₃- and H₂-loss were the exclusive channels found by ICR [21]. Insertion type fragmentation is exhibited by all of the Ln⁺ with promotion energies lower than that of Tm⁺ (i.e. <200 kJ mol⁻¹; Tm⁺ behaved in an intermediate fashion [21]), and results primarily in elimination of H₂, 2H₂, 3H₂, CH₄, {H₂,CH₄}, {2H₂,CH₄} and C₂H₆. Marçalo et al. [21] have rationalized the two types of fragmentation patterns in the context of the lanthanide ion energetics. The insertion type of activation mechanism occurs via

Table 2
Energetics for bare and oxo-ligated ions

M	Δ <i>E</i> [M ⁺] ^a	BDE[M ⁺ –O] ^b	IE[MO] ^c
Th	0 {5f ⁰ 6d ² 7s}	864	6.1
U	3 {5f ³ 7s ² → 5f ³ 6d7s}	796	5.6
La	0 {4f ⁰ 5d ² }	847	5.0
Ce	0 {4f ¹ 5d ² }	849	4.9
Pr	94 {4f ³ 6s → 4f ² 6d7s}	792	4.9
Nd	110 {4f ⁴ 6s → 4f ³ 5d ² }	749	5.0
Sm	258 {4f ⁶ 6s → 4f ⁵ 5d6s}	565	5.6
Gd	0 {4f ⁷ 5d6s}	732	5.8
Ta	0 {5d ³ 6s}	788	7.9

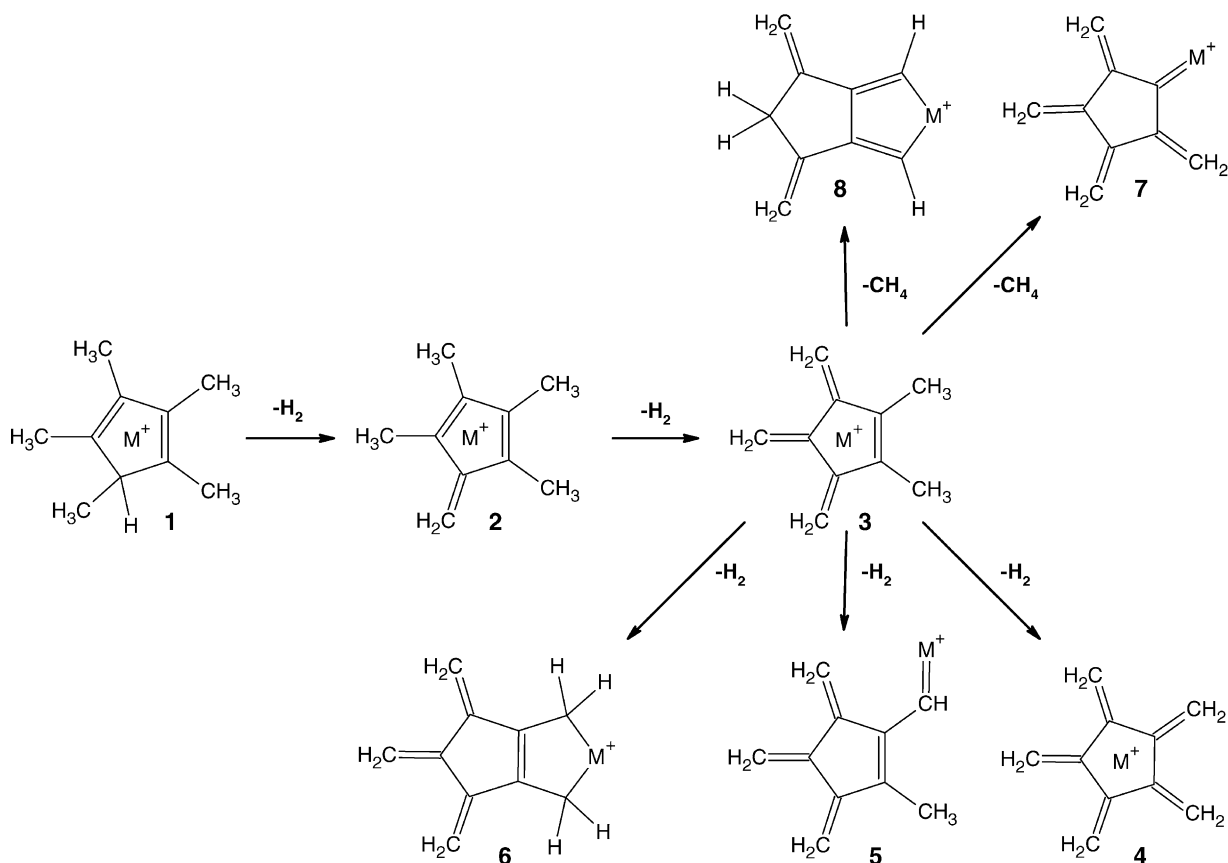
^a Promotion energy in kJ mol⁻¹ from the ground state to the lowest-lying electronic configuration with two non-f valence electrons. In the brackets, the ground state configuration is given where Δ*E* = 0; the ground and excited state configurations are given where Δ*E* > 0. The values for Th⁺ and U⁺ are from [33]; those for the Ln⁺ are from [34]; and that for Ta⁺ is from [35].

^b The oxide ion bond dissociation energies in kJ mol⁻¹ are from [36] (UO⁺, ThO⁺), [37] (LnO⁺) and [38] (TaO⁺).

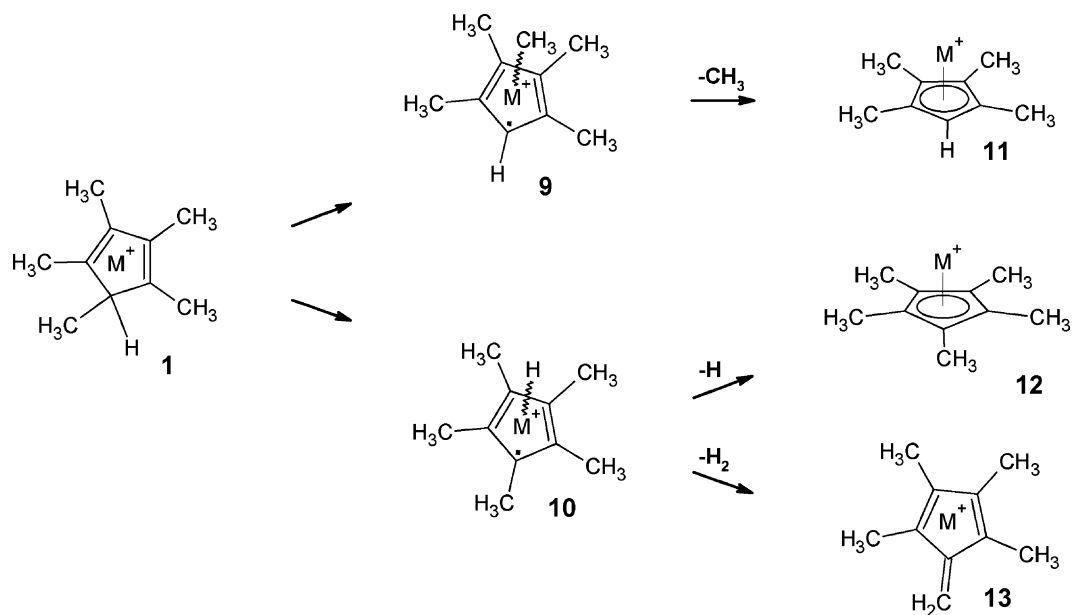
^c The oxide ion ionization energies (IE[MO] in eV, where 1 eV = 96.4 kJ mol⁻¹) are from [39,40]. These may not all be the most accurate available values for each of the MO, but were all measured in the same laboratory under similar conditions and should be precise to within ~0.2 eV for comparative purposes.

insertion of a metal ion into a C–H or C–C bond of a hydrocarbon; in the case of C–H activation, this can be represented by the following, where R represents a hydrocarbon backbone: $R-H + M^+ \rightarrow R-M^+-H$. This type of mechanism is presumed to account for the transformation of species **2** to **3** in Scheme 1. That this process proceeds for lanthanides and other metal ions, despite a presumably high barrier towards insertion, has been demonstrated and discussed elsewhere [7]. The mechanism corresponding to non-insertion activation of HCp^* and other molecules is more ambiguous and it was one of the goals of the present work to illuminate this issue. Those Ln^+ with prohibitively large promotion energies cannot effectively insert into hydrocarbon bonds, a presumption which had been well-established from studies of Ln^+ reactivity by

Cornehl et al. [7]. For the “non-insertion” Ln^+ , such as Sm^+ , it is proposed that activation instead occurs via a strong interaction of the metal ion with the π -system of HCp^* , which induces cleavage of the relatively weak C–CH₃ or C–H bond at the sp^3 carbon in the C₅-ring. Resulting activation of the C–C bond leads to loss of CH₃ and an Ln^+ -tetramethylcyclopentadienyl complex, $\{Ln^+ \cdot cyclo-C_5(CH_3)_4H\}$; alternatively, activation of the C–H bond can result in either H-loss and an Ln^+ -pentamethylcyclopentadienyl complex, $\{Ln^+ \cdot cyclo-C_5(CH_3)_5\}^+$; or subsequent β -H abstraction, H₂-loss, and an Ln^+ -tetramethylfulvene complex, $\{Ln^+ \cdot cyclo-C_5(CH_2)(CH_3)_4\}$ (these are structures **11–13** in Scheme 2). In contrast, activation by metal ion insertion into a C–H and/or C–C bond results in loss of one or more stable molecules, primarily



Scheme 1.



H_2 and CH_4 . This latter type of behavior is exhibited for all of the Ln^+ studied by QIT, with the exception of Sm^+ , as is evident from the results in Table 1.

From the QIT results in Table 1, it is seen that Th^+ exhibits a product distribution somewhat disparate from that exhibited by either the basic insertion or non-insertion mechanisms. The ground state configuration of Th^+ is quartet $6d^27s$ (Table 2), and this ion is expected to be more reactive than the Ln^+ . Ground state Th^+ should be even more reactive than the group IV d-block transition metal ion, Hf^+ , which has a doublet $5d6s^2$ ground state configuration and a quartet $5d^26s$ excited state configuration that is 44 kJ mol^{-1} higher in energy [35]. The very high reactivity of Th^+ has been previously demonstrated in its ability to exothermically dehydrogenate methane [12]; only the most reactive transition metal ions, including Ta^+ , have been shown to activate methane under thermoneutral conditions [1]. It is evident from previous results that Th^+ efficiently inserts into alkene C–H and C–C bonds, to enable dehydrogenation and cracking [12].

As is evident from Table 1, there is a conspicuous discrepancy in product distributions between Th^+ and the reactive group of Ln^+ , which includes La^+ , Ce^+ and Gd^+ ; the results for Ce^+ , the lanthanide homologue of Th^+ , from Marçalo et al. [21] indicate similar behavior to that of La^+ and Gd^+ . With regard to its electronic structure, Th^+ differs from the most reactive Ln^+ in that it has three, rather than only two, non-f valence electrons in its ground state. The chemistry of Th^+ with HCp^* was particularly distinctive in the appearance of the two channels corresponding to loss of $\{\text{H}_2, \text{H}\}$ and $\{\text{H}_2, \text{CH}_3\}$ (the latter might alternatively be reasonably formulated as $\{\text{CH}_4, \text{H}\}$). The behavior of Th^+ contrasts also with that of Ta^+ , which exhibits a variety of additional channels corresponding to a high degree of fragmentation, as is indicated in a footnote to Table 1. We postulate that the $\{\text{H}_2, \text{H}\}$ and $\{\text{H}_2, \text{CH}_3\}$ (and/or $\{\text{CH}_4, \text{H}\}$) elimination channels which are distinctive to Th^+ result in a complex in which the Th metal center is rendered inert towards further insertion processes, presumably due to participation of valence electron(s) in covalent

organometallic bonding with the resulting radical organic ligand. In contrast, Ta^+ , with its additional reactive valence electron— $5d^36s$ for ground Ta^+ vs. $6d^27s$ for ground Th^+ —evidently remains reactive, and induces additional H_2 -losses (e.g. $\{4\text{H}_2, \text{H}\}$). As noted below, the ionization energy of Ta is greater than that of HCp^* , and accordingly, electron transfer from HCp^* to Ta^+ is a competing process to associative reactions. The appearance of appreciable amounts of ionic reaction products which incorporate Ta reflects the highly reactive nature of both the HCp^* substrate, and the Ta^+ ion.

In the case of U^+ , the product distributions are qualitatively similar to those found with the reactive group of Ln^+ —i.e. primarily loss of one or more H_2 and/or CH_4 molecules. Significant quantitative discrepancies are evident in Table 1, for example, the much greater yield of the $\{3\text{H}_2\}$ -loss product in the case of uranium, but the results suggest essentially lanthanide-like behavior. In analogy with the lanthanides [7,21], it is concluded that U^+ activates HCp^* by a mechanism involving insertion of the metal ion into a C–H or C–C bond to form a C–U⁺–H or C–U⁺–C intermediate. The absence of the special types of reaction products seen for Th^+ or Ta^+ suggests that it is the outer valence d and s electrons of those two ions that enable their distinctive reaction pathways. The lanthanide-like behavior of U^+ superficially suggests that its 5f electrons, like the 4f electrons, do not play a significant role in the primary reaction mechanisms. As will become apparent from the ensuing discussion, the secondary reactions of U^+ and the behavior of UO^+ indicate that the character of uranium is indeed significantly different from that of the lanthanides. These differences are more clearly manifested in the reactions with HCp^* after the uranium metal center is bonded to a primary ligand. Although the results for bare U^+ are qualitatively similar to those for the Ln^+ , it should be noted that certain features of the product distributions in Table 1 do indeed suggest distinctive behavior for U^+ . For example, the 3H_2 -elimination channel is clearly more significant for U^+ than for the Ln^+ . It is feasible that such discrepancies between the primary product distributions may be related to 5f-effects in the case of ura-

nium, although the results summarized in Table 1 do not provide direct evidence for such an interpretation.

Charge exchange between HCp^* and the “reactant” ion competed with associative reactions for ions with ionization energies greater than that of HCp^* . Charge exchange to yield HCp^{*+} was observed for Ta^+ , Au^+ , TaO^+ , La^{2+} and Nd^{2+} (other M^{2+} were not produced in appreciable amounts). Among these ions, that with the smallest ionization energy is Ta: $\text{IE}[\text{Ta}] = 7.9 \text{ eV}$ [41] and charge exchange is consistent with the reported $\text{IE}[\text{HCp}^*]$ of 7.2 eV [41]. Electron transfer resulted primarily in HCp^{*+} at $m/z = 136$.

3.1.2. Secondary products

The secondary products are those resulting from the reaction of the primary $\text{M}[\text{HCp}^* - E]^+$ products, most of which are identified in Table 1, with a second HCp^* molecule. Because of the very disparate and complex product distributions for Ta^+ , these results are noted separately in a footnote to the table; this also applies to the results for TaO^+ . With regard to tantalum, the results for reactions of both Ta^+ and TaO^+ are not particularly enlightening, primarily demonstrating the highly reactive character of tantalum ions, and the particular susceptibility of the HCp^* substrate towards extensive fragmentation.

The net compositions of the secondary products are expressed as $\text{M}[(\text{HCp}^*)_2 - E]^+$, where $(\text{HCp}^*)_2$ corresponds to $\text{C}_{20}\text{H}_{32}$ and E is the postulated formulation of the net atomic losses from the two HCp^* molecules. The main secondary products are shown in Table 3, along with the corresponding ICR results for those Ln^+ that were also studied by the QIT approach. Because of the relatively low absolute yields of secondary products, which was due to the use of a low HCp^* pressure and short reaction times, the distributions are given as either observed, “+”, or absent, “–”. As a result of reduced sensitivity, some secondary products with yields of up to $\sim 10\%$ may not have been specified in Table 3.

As for the primary products, qualitative agreement is seen between the QIT and ICR results. In the case of Sm, the $\text{Sm}[(\text{HCp}^*)_2 - \text{H}]^+$ and $\text{Sm}[(\text{HCp}^*)_2 - \text{CH}_3]^+$ products are presumably adducts of the primary

Table 3
Secondary product distributions from reactions of bare metal ions with HCp*^a

<i>E</i> ^b	La ⁺	Pr ⁺	Nd ⁺	Sm ⁺	Gd ⁺	Th ⁺ ^c	U ⁺ ^c
H	–	–	–	–	–	–	–
CH ₃	–	–	–	–	–	–	–
H ₂	+	+	+	+	+	–	+
2H ₂	+	+	–	+	–	+	+
3H ₂	+	+	–	+	–	+	–
4H ₂	–	–	–	–	–	–	+
CH ₄	+	+	+	+	–	+	+
H ₂ ,CH ₄	+	+	–	+	–	+	+
2H ₂ ,CH ₄	–	–	–	–	–	+	–
H ₂ ,CH ₃	–	–	–	–	–	–	+
3H ₂ ,CH ₃	–	–	–	–	–	–	+

^a The results are expressed as either observed (+), or not detected (–) within the experimental sensitivity. The Ln⁺ results in the second column are from the ICR experiments of Marçalo et al. [21]. The QIT results for Ta⁺ were entirely distinctive, with the three major channels being net loss of {4H₂,H}, {5H₂}, and {6H₂}; 12 additional minor secondary products, several involving multiple C-loss, were identified for Ta⁺.

^b The products are {M[C₁₀H₁₆]₂ – *E*}⁺, where the eliminated moieties, *E*, are given.

^c Additional minor (≤10%) products were Th[(HCp*)₂ – {H₂, CH₄, H}]⁺, U[(HCp*)₂ – {3H₂, CH₄}]⁺, and U[(HCp*)₂ – {4H₂, CH₄}]⁺.

cyclopentadienyl product complexes, Sm[HCp* – H]⁺ and Sm[HCp* – CH₃]⁺. Marçalo et al. [20,21] concluded that the Sm[(HCp*)₂ – H₂]⁺ product corresponds to the samarocene sandwich complex, Cp* – Sm⁺ – Cp*. This samarocene could conceivably result from either the reaction of the primary Sm⁺ – Cp* product (i.e. Sm[HCp* – H]⁺) with HCp* and H-elimination, or rather by association of a fulvene reactant ion, Sm[HCp* – H₂]⁺, with a second HCp* followed by H-transfer between the ligands. The ICR results indicate that the more thermodynamically favorable association to the abundant fulvene product followed by rearrangement is the dominant pathway to the samarocene ion [20,21].

As with Sm⁺, the observed secondary product ions for the more reactive Ln⁺ are in qualitative agreement with the ICR results [21]. The primary difference is that some of the more highly fragmented secondary products, such as Pr[(HCp*)₂ – {3H₂}]⁺, were seen in the ICR but not in the QIT experiments. This distinction between the ICR vs. QIT experimental results is consistent with the primary product distributions, as discussed above. Comparison of the results in Tables 1 and 3 reveal that all of the major secondary products for the Ln correspond to compositions of primary products, with the addition of a second HCp*. It is not

obvious whether these addition products correspond to simple adducts or rather to rearrangement products.

The results in Table 3 reveal that the secondary product distribution for Th⁺ is distinctive from those for all of the other studied M⁺, in accord with the primary product results. The sensitivity to secondary products for Th⁺ was relatively poor, presumably due to a lower concentration of Th⁺ in the ion trap compared with most other metal ions. However, the two secondary products identified for Th⁺ in Table 3 were clearly dominant. These two products correspond to addition of a second HCp* molecule to the two most abundant primary products, Th[HCp* – {2H₂}]⁺ and Th[HCp* – {H₂, CH₃}]⁺. As with the Ln⁺, it appears that the Th⁺ metal center in the primary product ions is ineffective at activating a second HCp* molecule. Notably, this does not appear to be the case for Ta⁺. Whereas Ta[HCp* – {4H₂}]⁺ was a major primary product, and Ta[HCp* – {5H₂}]⁺ a minor primary product, both Ta[(HCp*)₂ – {5H₂}]⁺ and Ta[(HCp*)₂ – {6H₂}]⁺ were major secondary products, indicating activation of a second HCp* molecule by the Ta metal center in the primary products. This is consistent with the availability of an additional chemically active valence electron for Ta⁺ when compared with Th⁺.

Whereas the behavior for U^+ appeared at least qualitatively similar to that of the reactive group of Ln^+ regarding the primary product distributions, a significant discrepancy is evident in the secondary products. Among the primary products, $U[HCp^* - H_2]^+$ and $U[HCp^* - 3H_2]^+$, were the most abundant; the first of these is presumed to be a fulvene complex [20,21] and the second has been postulated to be a pentamethylenecyclopentane complex, $M^+ \cdot cyclo-C_5(CH_2)_5$ [22] (structures **2** and **4** in Scheme 1). The appearance of $U[(HCp^*)_2 - \{4H_2\}]^+$ as a major ($\sim 20\%$) secondary product suggests that the U metal center in one or more of the π -bonded primary complexes is able to activate and dehydrogenate a second HCp^* molecule. This is in distinct contrast to the Ln^+ and Th^+ primary products, for which only addition complexes appeared as secondary products. The distinctive appearance of $U[(HCp^*)_2 - \{4H_2\}]^+$ may reflect the large abundance of the presumed $U[HCp^* - \{3H_2\}]^+$ precursor (see Table 1). It is postulated that the metal center in this reactant complex ion can activate a second HCp^* molecule at the sp^3 carbon site in the C_5 ring, without direct insertion into the metal bond—this would then result in a fulvene as the second ligand. The high abundance of the triply-dehydrogenated precursor may be requisite for the appearance of the quadruply-dehydrogenated secondary product for U^+ . It would, nonetheless, appear that the electronic structure at the metal center in the primary uranium complex ions renders them more reactive than their lanthanide counterparts. For example, the lanthanide congener of uranium, neodymium, produces $Nd[HCp^* - H_2]^+$ as one of the two dominant primary products. Not only do sequential dehydrogenations of the initial HCp^* reactant molecule not occur with Nd^+ in the QIT, but reaction with a second HCp^* results in products corresponding only to net addition—the Nd^+ center is evidently ineffective at activating a second HCp^* molecule.

3.1.3. Reactions of mass-selected organouranium complex ions

Another secondary product that appeared for U^+ which did not correspond to addition to a primary

product was $U[(HCp^*)_2 - \{3H_2, CH_3\}]^+$. Both of the uranium secondary products which do not correspond to addition of a HCp^* molecule might have resulted from the reaction of the abundant $U[HCp^* - \{3H_2\}]^+$ primary product, via elimination of H_2 or CH_3 from the second HCp^* . Consistent with the triple-dehydrogenation product serving as the precursor for secondary products was the absence of the addition product, $U[(HCp^*)_2 - \{3H_2\}]^+$.

To clarify reaction pathways in the particularly intriguing and novel case of uranium, mass-selected chemistry of primary $U[HCp^* - E]^+$ product ions was carried out. As described in Section 2, a particular primary product ion could be isolated prior to reaction to identify specific secondary reaction pathways. The two requirements for this procedure are that the primary product be present in sufficient abundance to allow for its efficient isolation; and that the complex is sufficiently robust that the relatively minor kinetic (collisional) excitation due to resonant ejection of neighboring species does not result in its fragmentation.

Attempts were made to isolate the six major primary U^+ products identified in Table 1 for subsequent reaction. Neither $U[HCp^* - \{2H_2\}]^+$ nor $U[HCp^* - \{CH_4\}]^+$ could be isolated—it is concluded that these primary products were too fragile to allow selective ejection of neighboring ions. The susceptibility of $U[HCp^* - \{2H_2\}]^+$ towards loss of another H_2 molecule is consistent with the relative abundances of the single-, double- and triple- H_2 loss primary products: $U[HCp^* - H_2]^+$ and $U[HCp^* - \{3H_2\}]^+$ were clearly dominant (Table 1). It is notable that this contrasts with the product distributions for the reactive Ln^+ . Evidently, $U[HCp^* - \{2H_2\}]^+$ is substantially more susceptible to facile H_2 -elimination than are the $Ln[HCp^* - \{2H_2\}]^+$. The delicate nature of $U[HCp^* - \{CH_4\}]^+$ is also consistent with the lower yield of $U[HCp^* - \{CH_4\}]^+$ compared with the $Ln[HCp^* - \{CH_4\}]^+$ (Table 1).

It was possible to isolate the four other primary products of the reaction of U^+ with HCp^* . Both $U[HCp^* - H_2]^+$ and $U[HCp^* - \{H_2, CH_4\}]^+$ formed only the addition products, $U[(HCp^*)_2 - H_2]^+$ and

$U[(HCp^*)_2 - \{H_2, CH_4\}]^+$. Marçalo et al. [20,21] by ICR determined that the $Sm[(HCp^*)_2 - H_2]^+$ secondary product was the bis-pentamethylcyclopentadienyl complex, and by analogy we postulate that the first of these addition products in the case of uranium is the $Cp^*-\eta^5-U^+-\eta^5-Cp^*$ complex. This sandwich complex would result from H-atom transfer from a second HCp^* to a fulvene ligand. Postulated structures for the secondary $U[(HCp^*)_2 - \{H_2, CH_4\}]^+$ addition product are more speculative. However, a reasonable structure for the $[HCp^* - \{H_2, CH_4\}]$ ligand would be a fulvene that incorporates a cyclopropene moiety on one edge of the five-membered ring. The addition of a second HCp^* to such a structure could then result in a $Cp^*-\eta^5-U^+-\eta^5-[HCp^* - \{H, CH_4\}]$ product in which both of the ligands are aromatic upon electron donation from the uranium metal center.

A second distinctive pattern of secondary reactions was seen with the other two isolated primary products, $U[HCp^* - \{3H_2\}]^+$ and $U[HCp^* - \{2H_2, CH_4\}]^+$. For both, the main secondary reactions were loss of H_2 or CH_3 . Incidentally, the absence of $U[(HCp^*)_2 - \{2H_2, CH_4, CH_3\}]^+$ in Table 3 can be attributed to the relatively low abundance of the $U[HCp^* - \{2H_2, CH_4\}]^+$ precursor (Table 1). As is seen in Table 1, the H_2 - and CH_3 -elimination channels are precisely those that are dominant for bare Sm^+ , one of the group of lanthanide ions that react with HCp^* via a non-insertion mechanism which results in activation at the sp^3 carbon. The uranium results indicate that the uranium metal center in these two primary products is ineffective at direct insertion into C–H or C–C bonds, suggesting that the two chemically active non-5f valence electrons are engaged in covalent bonding and that the 5f electrons remaining at the metal center are essentially inert towards organometallic reactions that require insertion into a C–H or C–C bond. This interpretation is substantiated by the close similarity between the reactions of $U[HCp^* - \{3H_2\}]^+$ and $U[HCp^* - \{2H_2, CH_4\}]^+$ to those of the uranium monoxide ion, $U^+=O$, as discussed below. Based on these results we postulate structures for the two reactant uranium complex ions which exhibit the non-insertion, Sm^+ type of behav-

ior. Specifically, we conclude that the uranium forms two covalent bonds, in which the two available non-5f valence electrons are chemically engaged. This conclusion is summarized in Scheme 1 where postulated reaction sequences leading to $U[HCp^* - \{3H_2\}]^+$ and $U[HCp^* - \{2H_2, CH_4\}]^+$ are shown. Because the uranium metal center evidently remains chemically active after the loss of two H_2 molecules, the π -bonded structure **3** would seem a reasonable intermediate for both products ($M^+ = U^+$ in Scheme 1). Subsequent loss of a third H_2 molecule was previously [22] postulated to result in the π -bonded structure **4** for the lanthanides ($M^+ = Ln^+$). However, the present results for uranium point towards a structure with two covalent organometallic bonds. Two structures that fulfill this condition are **5** and **6**. Structure **6** would seem the more reasonable of the two based upon both mechanistic and thermodynamic considerations. Mechanistically, the U^+ in structure **3** ($M^+ = U^+$) could readily bridge the methyl groups with concomitant loss of H_2 , and thermodynamically, the resulting structure **6** retains a fully conjugated π -system. The availability of the process leading from **3** to **6** may well account for the low abundance of the $U[HCp^* - \{2H_2\}]^+$ product and its particular susceptibility towards off-resonance fragmentation. An analogous process should be available for structure **2**, the presumed single-dehydrogenation product. That this latter process evidently does not readily occur suggests that **2** is particularly stable, this in accord with a thermodynamic analysis presented below. As for $U[HCp^* - \{3H_2\}]^+$, the Sm^+ -like (and UO^+ -like) character of the uranium metal center in $U[HCp^* - \{2H_2, CH_4\}]^+$ suggests structures such as **7** and **8** ($M^+ = U^+$), both of which incorporate two covalent uranium bonds. Alternative structures resulting from fracture of the C_5 -ring are feasible but considered mechanistically and thermodynamically less likely. Formation of structure **8** via CH_4 -loss from **3** would require considerable rearrangements and is considered rather unlikely; instead, structure **7** is considered the more feasible of the two. Although structures **6** and **7** are considered probable structures for the distinctive uranium complex ions, it is emphasized

that we have no evidence for these particular configurations. The key conclusion is that there are two covalent uranium–carbon organometallic bonds in the two primary products, be they of an alkyl- or carbene-type character.

The QIT results for uranium contrast with those for the reactive lanthanides (i.e. those Ln^+ which activate via insertion). Specifically, secondary reactions of $\text{Ln}[\text{HCp}^* - \{3\text{H}_2\}]^+$ and $\text{Ln}[\text{HCp}^* - \{2\text{H}_2, \text{CH}_4\}]^+$ resulted only in association products—no loss of H_2 or CH_3 was seen [21]. It would appear that the metal center in the uranium primary products remains chemically active towards non-insertion activation of a second HCp^* molecule whereas the lanthanide metal centers in the corresponding primary products are effectively inert. If the $\text{Ln}[\text{HCp}^* - \{3\text{H}_2\}]^+$ and $\text{Ln}[\text{HCp}^* - \{2\text{H}_2, \text{CH}_4\}]^+$ products can be represented by structures such as **6** and **7** shown in Scheme 1, the trivalent lanthanide metal center would indeed be valence saturated and chemically inert. In contrast, the uranium metal centers in these structures have three non-bonded valence electrons, presumably of predominantly 5f-character. The results for the two distinctive uranium complex ions suggest that non-insertion activation of HCp^* by bare metal ions such as Sm^+ requires participation of a valence electron, and does not proceed by a simple electrostatic interaction. This conclusion is more definitively supported by the results for ThO^+ and UO^+ , discussed below. We can exclude structure **4** as being significant

for uranium but do not have direct evidence that triple dehydrogenation of HCp^* by Ln^+ results in a covalently bonded organometallic complex. The gas-phase organometallic chemistry of Ln^+ may be entirely distinctive from that of U^+ as a result of the inert character of the lanthanide 4f electrons, and results from this study clearly demonstrate a distinctive chemical behavior of uranium compared with that of the lanthanides.

3.2. Reactions of MO^+ (and UO_2^+) with HCp^*

3.2.1. Primary products

The product distributions for reactions of the oxo-ligated metal ions, MO^+ , with HCp^* are given in Table 4. The relevant ICR results for lanthanide ions are again included for comparison [21]. As with the primary products, there is general agreement between the ICR and QIT product distributions for the studied lanthanides. The main discrepancy was the generally greater yields of the association complexes in the QIT experiments. This contrast is consistent with the greater degree of fragmentation found for the bare Ln^+ and is attributed to the differences in experimental conditions, as discussed below. For all of the LnO^+ , the association product was the dominant product in the QIT experiments. As discussed by Marçalo et al. [21], these products may correspond to $\text{O}=\text{M}^+-\text{HCp}^*$, or to $\text{HO}-\text{M}^+-\text{Cp}^*$, in both of which the metal center is trivalent.

Table 4
Primary product distributions from reactions of metal oxide ions with HCp^* ^a

E^b	LaO^+	PrO^+	NdO^+	SmO^+	GdO^+	ThO^+	UO^+					
–	100	<i>100</i>	100	<i>100</i>	100	<i>100</i>	67	10	62	<i>10</i>	–	–
H	–	–	–	–	–	–	–	–	–	–	7	–
CH_3	–	–	–	–	–	–	–	–	–	–	60	45
H_2	–	–	–	–	–	–	–	14	11	17	30	50
H_2O	–	–	–	–	–	–	33	76	20	65	–	–

^a The values are percentages of the total yield of all secondary products. The precision (variation between experiments) for the minor products (<10% yield) was within a factor of 2. The cited values for the major products ($\geq 10\%$) were reproducible to within ± 5 . For each of the lanthanides, the italicized values are from the ICR experiments of Marçalo et al. [21]. Non-observed products are designated by a “–”. The results for TaO^+ were entirely distinctive, with the major channels being net loss of $\{2\text{H}_2\}$ (11%); $\{3\text{H}_2\}$ (44%); and $\{3\text{H}_2, \text{CH}_4\}$ (15%); four additional minor secondary products were identified for TaO^+ .

^b The products are $\{\text{MO}[\text{C}_{10}\text{H}_{16}] - E\}^+$, where the eliminated moieties, E , are given.

For several LnO^+ , H_2O -elimination was a significant channel, and proceeds according to the reaction shown in Eq. (1).



In analogy with the corresponding products which result from Ln^+ -induced dehydrogenation of HCp^* , it is presumed that the organometallic product of Eq. (1) is an Ln^+ -tetramethylfulvene complex, structure **2** in Scheme 1. Because this reaction requires the cleavage of the Ln^+ -O bond, it proceeds exothermically only for those LnO^+ with relatively small bond dissociation energies, $\text{BDE}[\text{Ln}^+-\text{O}]$. This dehydration reaction was observed for SmO^+ and GdO^+ by both QIT (Table 4) and ICR [21]— GdO^+ is the LnO^+ with the largest $\text{BDE}[\text{Ln}^+-\text{O}]$ for which reaction (1) was observed by ICR [21]. Although the thermochemistry of HCp^* is not well-established, Lias et al. [38] have estimated $\Delta_f\text{H}[\text{methylcyclopentadiene}] \approx 96 \text{ kJ mol}^{-1}$. Using this value with the known thermochemistry for fulvene [38] gives an estimated enthalpy of 128 kJ mol^{-1} for the dehydrogenation of methylcyclopentadiene to give fulvene; this can also be taken as an approximation for the enthalpy of dehydrogenation of HCp^* to give tetramethylfulvene. Using $\Delta_f\text{H}[\text{H}_2\text{O}] = -242 \text{ kJ mol}^{-1}$, $\Delta_f\text{H}[\text{O}] = 249 \text{ kJ mol}^{-1}$ [28] and $\text{BDE}[\text{Gd}^+-\text{O}] = 732 \text{ kJ mol}^{-1}$ [37], for reaction (1) to proceed exothermically for GdO^+ would require that $\text{BDE}[\text{Gd}^+-\text{HCp}^* - \text{H}_2]$ be at least $\sim 369 \text{ kJ mol}^{-1}$. This would be an unusually strong bond between a metal ion and an organic π -system; for comparison the Ti^+ -benzene bond is among the strongest known of this type and $\text{BDE}[\text{Ti}^+-\text{C}_6\text{H}_6] = 263 \text{ kJ mol}^{-1}$ [2]. The anomalously strong bonding inferred from this analysis suggests that the bonding in the $\text{Ln}[\text{HCp}^* - \text{H}_2]^+$ species may involve substantial disruption of bonding in the fulvene ligand, and some contribution from covalent organometallic bonding. We will continue to refer to the $[\text{HCp}^* - \text{H}_2]$ ligand as a fulvene (i.e. structure **2**), with the implicit caveat of the potential for substantial deviation from this simplistic description. That reaction (1) evidently does not proceed for NdO^+ or any LnO^+ with greater BDEs than

$\text{BDE}[\text{Nd}^+-\text{O}] = 749 \text{ kJ mol}^{-1}$ suggests an upper limit for $\text{BDE}[\text{Ln}^+-\text{HCp}^* - \text{H}_2]$ of $\sim 386 \text{ kJ mol}^{-1}$.

The chemistries of ThO^+ , UO^+ and TaO^+ were entirely distinctive from those of the LnO^+ . In assessing the comparative behaviors of the MO^+ , it is useful to consider the effects of oxo-ligation on metal ion chemistry, as has been discussed in a broad context by Schröder et al. [42]. More specifically, Cornehl et al. [8] have examined reactions of LnO^+ with alkenes and found a correlation between the electron affinity of the monoxide ion and its reactivity. With butadiene, DyO^+ ($\text{IE}[\text{DyO}] = 6.1 \text{ eV}$) was nearly inert ($k/k_{\text{ADO}} = 0.01$) whereas TmO^+ ($\text{IE}[\text{TmO}] = 6.4 \text{ eV}$) was highly reactive ($k/k_{\text{ADO}} = 1.0$). A remarkably dramatic enhancement in reactivity was evidently induced by increasing the oxide ion electron affinity by only $\sim 0.3 \text{ eV}$. These authors postulated a non-insertion mechanism that proceeds via electrophilic attack of the metal oxide ion on the π -system of the alkene. In accord with this hypothesis, the reactivity onset was shifted to lower $\text{IE}[\text{LnO}]$ when the more nucleophilic isoprene substrate was employed [8]. The HCp^* molecule, with its ionization energy of only 7.2 eV [41], should be especially susceptible to such electrophilic attack by metal oxide ions. To assess the possible role of this effect in the chemistries of the examined MO^+ , we consider the self-consistent ionization energies obtained by Ackermann et al. by the electron impact method which are compiled in [40] and included in Table 2: $\text{IE}[\text{LaO}] \approx \text{IE}[\text{PrO}] \approx \text{IE}[\text{NdO}] \approx 5.0 \text{ eV}$; $\text{IE}[\text{SmO}] \approx \text{IE}[\text{UO}] \approx 5.6 \text{ eV}$; $\text{IE}[\text{GdO}] \approx 5.8 \text{ eV}$; $\text{IE}[\text{ThO}] \approx 6.1 \text{ eV}$; and $\text{IE}[\text{TaO}] \approx 7.9 \text{ eV}$. In view of the large $\text{IE}[\text{TaO}]$, the extreme reactivity of TaO^+ might be due to its high electron affinity and resultant electrophilic attack on HCp^* . As noted above, the higher ionization energy of TaO compared with HCp^* results in charge transfer as a competing process to associative reactions. Although the particularly high electron affinity of TaO^+ likely has a significant effect on its reactivity with HCp^* , the two chemically active 5d valence electrons at the metal center in TaO^+ might also contribute to the substantial fragmentation of the HCp^* ligand. In contrast, the electron affinity of UO^+ is evidently less than that of GdO^+ , and that of ThO^+

is only slightly greater than that of GdO^+ . Although an electrophilic attack mechanism could conceivably account for an enhanced reactivity of ThO^+ , it would not be expected that the product distributions would be affected in the manner observed. Specifically, the appearance of channels corresponding to elimination of H and CH_3 exclusively for ThO^+ and UO^+ indicates unique chemistry for these two MO^+ . It is concluded that the distinctive product distributions for ThO^+ and UO^+ are due to the electronic structures at the metal centers, and not the electron affinities of the metal oxide ions.

Comparing Tables 1 and 4, it is apparent that the product distributions for ThO^+ and UO^+ are very similar to those for the “non-insertion” lanthanide ion, Sm^+ . The $\text{UO}[\text{HCp}^* - \text{H}]^+$ product was not detected to within the limited sensitivity of these experiments, but was also only a minor product for ThO^+ and Sm^+ , as well as the other Sm^+ -like lanthanides studied by ICR [21]. In the case of Tm^+ , the ICR yield of $\text{Tm}[\text{HCp}^* - \text{H}]^+$ was only 2% [21], which is below the sensitivity of the present QIT experiments. Accordingly the lack of detectable $\text{UO}[\text{HCp}^* - \text{H}]^+$ is not taken to indicate particularly distinctive behavior for UO^+ . No LnO^+ ions induce elimination of H or CH_3 from HCp^* [21]. The trivalent metal centers in the LnO^+ have no additional valence electrons that can readily participate in bonding. It is concluded that the mechanisms that result in the product distributions distinctive to Sm^+ , Eu^+ , Tm^+ , Yb^+ , Ca^+ , Sr^+ , Ba^+ , ThO^+ and UO^+ require a chemically active valence electron at the metal center that can participate in the activation process. A postulated mechanism for the M^+ -induced elimination of CH_3 , H and H_2 is shown in Scheme 2, where M^+ represents a bare metal ion such as Sm^+ that exhibits this type of reactivity, one of the actinide oxides, ThO^+ and UO^+ , or one of the primary products, $\text{U}[\text{HCp}^* - \{3\text{H}_2\}]^+$ and $\text{U}[\text{HCp}^* - \{2\text{H}_2, \text{CH}_4\}]^+$. We postulate that the interaction of cations such as these with the HCp^* substrate results in abstraction of the relatively weakly bound CH_3 or H ligand at the sp^3 carbon. Based on the apparent necessity for a chemically active valence electron at the metal center, we propose that these abstractions

result in the intermediates **9** and **10**, in which there is some covalent bonding interaction between the metal center and either the CH_3 radical or the H atom. Structure **9** is one isomer—the radical center could alternatively be at one of the four methylated carbon sites; similarly, there are five resonance structures for **10**. Elimination of the CH_3 radical from **9** would then result in product **11**, a tetramethylcyclopentadienylidene complex; elimination of an H atom from **10** would result in product **12**, a pentmethylcyclopentadienylidene complex; and elimination of a H_2 molecule via β -H abstraction would result in product **13**, a tetramethylfulvene complex. The low abundance of **12** for all of the reactions of this type suggests β -H abstraction as the favored pathway for the intermediate **10**. Although the charge on the metal or metal oxide is given as +1 in products **11** and **12** in Scheme 2, the actual charge distribution is indeterminate. The representation of η^5 bonding between the ion and the aromatic cyclopentadienylidene complexes in **11** and **12** implies charge transfer from the metal center to the cyclopentadienyl ring, which is formally the aromatic anion, Cp^{*-} , in condensed phase f-block cyclopentadienylidene complexes [43]. The bonding between the ion, M^+ , and the π -ligands in the initial association complex as well as the intermediates **9** and **10** and the fulvene product **13** is presumably primarily via interaction with the conjugated diene π -system, and not as robust as between the ion and the cyclopentadienyl ligands. For comparison, $\text{BDE}[\text{Fe}^+ - \text{Cp}] = 368(29) \text{ kJ mol}^{-1}$ vs. $\text{BDE}[\text{Fe}^+ - \text{HCp}] = 230(21) \text{ kJ mol}^{-1}$ [44], where HCp represents the unsubstituted cyclopentadiene ligand. Products **11** and **12** are stabilized by the strong interaction between the ion and the Cp^* ligand, and product **13** (as well as **2** in Scheme 1) is stabilized by the fully conjugated π -system in the fulvene ligand. However, as discussed above in the context of the observed GdO^+ chemistry with HCp^* , the description of the bonding in structure **13** is likely more complex than suggested by this structure; the bond strength between the metal ion and the ligand is evidently comparable to that between metal ions and Cp^* .

The inability of lanthanide ions such as Sm^+ to activate alkenes via insertion mechanisms has been

rationalized based on the large energies ($\geq 200 \text{ kJ mol}^{-1}$) needed to excite from the ground state to an electronic configuration, $4f^{n-2}5d6s$, with two non-4f valence electrons available for participation in covalent bonding [7]. The ground states of each of the Ln^+ which exhibit the HCp^* fragmentation pattern exhibited by Sm^+ is $4f^{n-1}6s$ [34], so that there is a valence 6s electron available to form the single bond in the postulated intermediates, **9** and **10**. For ThO^+ and UO^+ , two valence electrons at the metal center are engaged in the strong $\text{M}^+=\text{O}$ bonds. Accordingly, a third valence electron must be available at the metal center to enable the mechanism postulated in Scheme 2. The energies necessary to achieve an electronic configuration for M^+ with a valence d^2s or d^3 configuration range from zero for Th^+ and Ta^+ (see the ground state configurations in Table 2) to 189 kJ mol^{-1} for U^+ [33], 389 kJ mol^{-1} for Ce^+ , and much larger, chemically inaccessible, values for all of the other Ln^+ [34]. The implied large promotion energies for the metal centers in all LnO^+ is consistent with their inability to activate HCp^* according to Scheme 2. The nature of the metal center in LnO^+ has been discussed in this context by Cornehl et al. [9]. In the case of TaO^+ , the availability of two chemically active valence electrons at the metal center results in a high reactivity via the typical insertion-type mechanism, with loss of molecular hydrogen and methane. The $6d^27s$ ground state of Th^+ would suggest that one non-5f valence electron remains at the metal center in ThO^+ , consistent with the observed Sm^+ -like behavior and the mechanism in Scheme 2.

The results for UO^+ are particularly interesting in that Sm^+ -like behavior suggests a chemically active electron at the metal center. In a comparative study of the gas-phase chemistry of NdO^+ and UO^+ , Cornehl et al. [9] attributed the greater dehydrogenation activity of UO^+ to direct participation of two 5f electrons at the metal center in alkene activation. The present results also imply that the metal center in UO^+ remains chemically active. However, the observed behavior towards activation of HCp^* suggests that the chemistry with this reaction substrate is dominated by processes which require only one chemically active valence

electron. Furthermore, it cannot be confidently deduced from the present results whether this valence bonding electron is of predominately 5f character, in a hybrid 5f/6d/7s orbital, or even in a (high energy) orbital of predominantly 6d or 7s character. However, based on the results of calculations on the electronic structure of UO^+ , Cornehl et al. [9] concluded that the remaining 5f electrons at the metal center in UO^+ were indeed of 5f character. The distinctive behavior of UO^+ in the present work would appear to provide particularly convincing evidence for a role of the 5f electrons of uranium in organometallic bonding.

As was noted above, the chemistry of the two primary products for reactions of bare U^+ , $\text{U}[\text{HCp}^* - \{3\text{H}_2\}]^+$ and $\text{U}[\text{HCp}^* - \{2\text{H}_2, \text{CH}_4^+\}]^+$, was very similar to that of UO^+ (and Sm^+). It was based on this comparison that structures such as **5–8** in Scheme 1—i.e. covalently bonded U^+ —were deduced. Because two valence electrons at the metal center in UO^+ are engaged in the uranium–oxygen double bond, it can be inferred that two valence electrons are similarly engaged in bonding in the organometallic complex ions that exhibit essentially the same chemistry as UO^+ .

The only dioxide ion produced in sufficient abundance to study was UO_2^+ . The two products of its reaction with HCp^* were the mono- and bis-addition products, $\text{UO}_2^+\cdot\text{HCp}^*$ and $\text{UO}_2^+\cdot 2\text{HCp}^*$. After long reaction times, conversion to $\text{UO}_2^+\cdot 2\text{HCp}^*$ was complete. The formation of addition products without elimination reactions is consistent with a sole low-energy localized 5f electron remaining at the metal center in UO_2^+ [9]. The formulation of the addition products as the adducts, $\text{UO}_2^+\cdot\text{HCp}^*$ and $\text{UO}_2^+\cdot 2\text{HCp}^*$, may not be the most reasonable. Rearrangement via the type of H-transfer exhibited in the reaction, $\{\text{Sm}[\text{HCp}^* - \text{H}_2]^+ + \text{HCp}^* \rightarrow \text{Sm}[(\text{HCp}^*)_2 - \text{H}_2]^+\}$ [21], is also feasible for the UO_2^+ addition reactions. Alternative formulations for $\text{UO}_2^+\cdot 2\text{HCp}^*$ which would result from H-transfer from HCp^* to one or both oxygen ligands are $\{\text{UO}(\text{OH})\text{Cp}^*\cdot\text{HCp}^*\}^+$ and $\{\text{U}(\text{OH})_2\text{Cp}^*_2\}^+$. These pentamethylcyclopentadienylidene hydroxide species would retain the robust uranium–oxygen bonding and introduce strong U^+-Cp^* bonding, and are likely

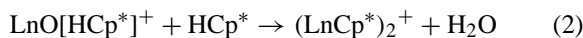
the thermodynamically favored products. A species such as $\{\text{U}(\text{OH})_2\text{Cp}^*_2\}^+$ is analogous to well-known condensed phase organouranium complexes such as Cp_2UCl_2 [43]. However, in contrast to the prevalent tetravalent uranium organometallic complexes commonly found in the condensed phase [43], the uranium metal center is in a formally pentavalent state in each of the three gas-phase isomers: $\{\text{O}=\text{U}^+=\text{O}\}\cdot 2\text{HCp}^*$; $\{\text{Cp}^*(\text{OH})\text{U}^+=\text{O}\}\cdot \text{HCp}^*$; and $\text{Cp}^*_2\text{U}^+(\text{OH})_2$.

The absence of the Sm^+ -type reaction products for UO_2^+ , in contrast to UO^+ , supports the theory that a chemically active valence electron is necessary for the non-insertion reactions, and the reaction mechanisms postulated in Scheme 2. In essence, UO_2^+ behaves in a similar manner to the inert LnO^+ , such as PrO^+ , with regard to association as the sole primary reaction channel. However, addition of a second HCp^* molecule to $\text{UO}_2^+\cdot\text{HCp}^*$, contrasts with the secondary reaction channels for LnO^+ , as discussed in Section 3.2.2. The formation of appreciable amounts of UO_2^+ , and its subsequent reactions, is attributable to accessible oxidation states above III, this in contrast to the predominantly trivalent chemistry exhibited by the lanthanides. That neither UO^+ nor UO_2^+ react with HCp^* via dehydration reflects the large $\text{BDE}[\text{U}^+-\text{O}] = 796 \text{ kJ mol}^{-1}$ and $\text{BDE}[\text{OU}^+-\text{O}] = 776 \text{ kJ mol}^{-1}$ [36].

3.2.2. Secondary products

The secondary products from reactions of the monoxide ions with HCp^* are indicated in Table 5, along with the ICR results for these lanthanides from

Marçalo et al. [21]. For each LnO^+ , the only observed product corresponded to H_2O -elimination. The results are consistent with the ICR results [21], where the products of the primary “adducts” reacting with a second HCp^* corresponded to H_2O -elimination. In the ICR experiments with SmO^+ and GdO^+ , an additional secondary product corresponding to net loss of $\{\text{H}_2, \text{H}_2\text{O}\}$ resulted from elimination of H_2 from a second HCp^* induced by the dominant primary product, $\text{Ln}[\text{HCp}^* - \text{H}_2\text{O}]^+$. Using CID, Marçalo et al. [21] demonstrated that the $\text{PrO}[(\text{HCp}^*)_2 - \text{H}_2\text{O}]^+$ product is the bis-cyclopentadienyl sandwich complex, $\text{Cp}^*-\eta^5-\text{Pr}^+-\eta^5-\text{Cp}^*$. Reaction (2) is driven by the strong organometallic bond between the metal center and the Cp^* ligands, and by the stability of the eliminated water molecule.



In contrast to Eq. (1), the organometallic dehydration product of Eq. (2) incorporates strong bonding between the metal center and two radical Cp^* ligands. Accordingly, whereas substantial yields of the primary $\text{LnO}[\text{HCp}^* - \text{H}_2\text{O}]^+$ appeared only for the more weakly bound LnO^+ , H_2O -loss was the dominant secondary reaction for even the most strongly bound LnO^+ .

For ThO^+ and UO^+ , the secondary products correspond to addition of a second HCp^* molecule to the primary products. These results are considered in the context of the proposed structures 11–13 in Scheme 2 for the primary reaction products. With one exception,

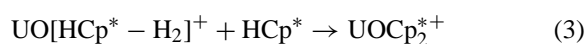
Table 5
Secondary product distributions from reactions of metal oxide ions with HCp^* ^a

<i>E</i> ^b	LaO^+		PrO^+		NdO^+		SmO^+		GdO^+		ThO^+	UO^+
H	–	–	–	–	–	–	–	–	–	–	+	–
CH_3	–	–	–	–	–	–	–	–	–	–	+	+
H_2	–	–	–	–	–	–	–	–	–	–	+	+
H_2O	+	+	+	+	+	+	+	+	+	+	–	–

^a The results are expressed as either observed (+), or not detected (–) within the experimental sensitivity. The Ln^+ results in the second column are from the ICR experiments of Marçalo et al. [21]. A minor additional product for GdO^+ corresponded to net loss of $\{\text{H}_2, \text{H}_2\text{O}\}$. The results for TaO^+ were entirely distinctive, with none of the AnO^+ nor LnO^+ products in evidence. The major channels for TaO^+ were net loss of $\{3\text{H}_2\}$, $\{4\text{H}_2\}$, $\{3\text{H}_2, \text{CH}_4\}$, $\{4\text{H}_2, \text{CH}_4\}$, and $\{4\text{H}_2, \text{C}_2\text{H}_6\}$; five additional minor secondary products were identified for TaO^+ .

^b The products are $\{\text{MO}[\text{C}_{10}\text{H}_{16}]_2 - E\}^+$, where the eliminated moieties, *E*, are given.

the addition products are considered to be adducts of a second HCp* to these primary products, where M = ThO⁺ and UO⁺. Whereas the addition of HCp* to the two abundant primary products, **11** and **13**, occurred with comparable efficiencies for ThO⁺, the addition of a second HCp* was more efficient for UO[HCp* – H₂]⁺ compared with UO[HCp* – CH₃]⁺. In analogy with the conclusion by Marçalo et al. [21] that the product of addition of an HCp* to the Ln⁺–fulvene product results in (LnCp*)₂⁺, we propose that addition of HCp* to UO[HCp* – H₂]⁺ occurs according to Eq. (3).



This corresponds to the transfer of an H-atom from the second HCp* molecule to the fulvene ligand, and a UOCp*₂⁺ addition product in which a formally pentavalent uranium metal ion center is bonded to an O-atom and two Cp* ligands: O=U⁺(Cp*)₂. Because this process results in a pentavalent metal center, an oxidation state that is effectively inaccessible for Th, the analogous process is not feasible for ThO⁺. This is in accord with the comparable efficiencies observed for addition of HCp* to ThO[HCp* – CH₃]⁺ and ThO[HCp* – H₂]⁺ to produce simple adducts.

As noted in a footnote to Table 5, a small amount of GdO[(HCp*)₂ – {H₂, H₂O}]⁺ was seen as a secondary product. This is consistent with the ICR results [21], where the primary Gd[HCp* – H₂]⁺ product reacts with a second HCp* molecule to eliminate water. This channel accounts for the absence of the GdO[(HCp*)₂ – H₂]⁺ addition product in the present study.

3.3. Collision-induced dissociation and variable bath gas pressures

Although the QIT results for lanthanide ions are in qualitative agreement with the ICR results, there are significant discrepancies between the product distributions. In attempting to understand the origins of these differences, we focused on effects of experimental parameters on the product distributions in the particular case of the primary reactions of La⁺ with HCp*.

Referring to Table 1, it is evident that a substantially greater degree of fragmentation occurred under the ICR conditions [21]. In the particular case of La⁺, H₂- and CH₄-elimination were the dominant channels under the QIT conditions. Under the ICR conditions, elimination of one or two additional H₂ molecules were substantially more important pathways; loss of C₂H₆ was even a significant channel in ICR. To explore the nature of these discrepancies, a mass-selected {Ln⁺ + HCp*} primary product was subjected to resonant excitation to induce collision-induced dissociation (CID). Also, product distributions for the {La⁺ + HCp*} reaction were monitored as a function of the bath gas pressure in the QIT.

3.3.1. Collision-induced dissociation

CID of an isolated complex ion, La[HCp* – H₂]⁺, was carried out according to the procedure described in Section 2. CID of organic ions in a QIT using He as the bath gas has been described [28,45]. For organic ions, a correlation between the threshold resonance excitation amplitude applied to the ion and the known decomposition energies was revealed. Although the relationships between ion excitation and dissociation remain empirical, it is evident that the extent of excitation and resultant dissociation exhibit a direct correlation. As noted by McLuckey and Goeringer [46], the multi-collision excitation process in QIT CID is slow relative to dissociation. Accordingly, the CID process can be envisioned as heating of the complex ion. There is a close analogy between complex ion CID in the QIT and the Infrared Multiphoton Dissociation process that was pioneered by Dunbar [47].

In Fig. 1 are shown the mass spectra for excitation of the La[HCp* – H₂]⁺ complex using excitation voltages of 100, 180 and 600 mV_{p-p}, each applied for 20 ms. The peak at *m/z* = 274 is where an La[HCp* – H]⁺ product would appear, but its intensity is sufficiently close to the 11% expected for La[¹²C₉¹³CH₁₄]⁺ that it is considered to be this isotopologue of La[HCp* – H₂]⁺. Because this minor ¹³C isotopologue ion was not resonantly excited, it did not exhibit the same fragmentation behavior as the main La[¹²C₁₀H₁₄]⁺ isotopologue in the CID experiments.

The onset of fragmentation of $\text{La}[\text{HCp}^* - \text{H}_2]^+$ occurred for excitation voltages in the region of $\sim 120 \text{ mV}_{\text{p-p}}$. No bare La^+ resulted from CID of $\text{La}[\text{HCp}^* - \text{H}_2]^+$; instead, collisional heating leads to loss of additional H_2 , CH_4 , and/or C_2H_6 molecules. Near the dissociation threshold, the abundances of $\text{La}[\text{HCp}^* - 2\text{H}_2]^+$ and $\text{La}[\text{HCp}^* - 3\text{H}_2]^+$ were comparable; at higher energies the latter was dominant (spectrum B in Fig. 1). At even higher excitation, additional H_2 -losses and C–C bond cleavages were seen (spectrum C in Fig. 1).

The CID results shown in Fig. 1 demonstrate that collisional excitation of organometallic complexes in the QIT do not serve to directly illuminate structures or bonding in a complex ion such as $\text{La}[\text{HCp}^* - \text{H}_2]^+$. Rather, it would appear that multi-collisional CID in the QIT results in relatively gradual heating of the complex which effectively pyrolyzes the composite ligand. The greater degree of fragmentation associated with resonant excitation appears similar to the distinctive product abundances associated with the ICR as compared with the QIT experiments.

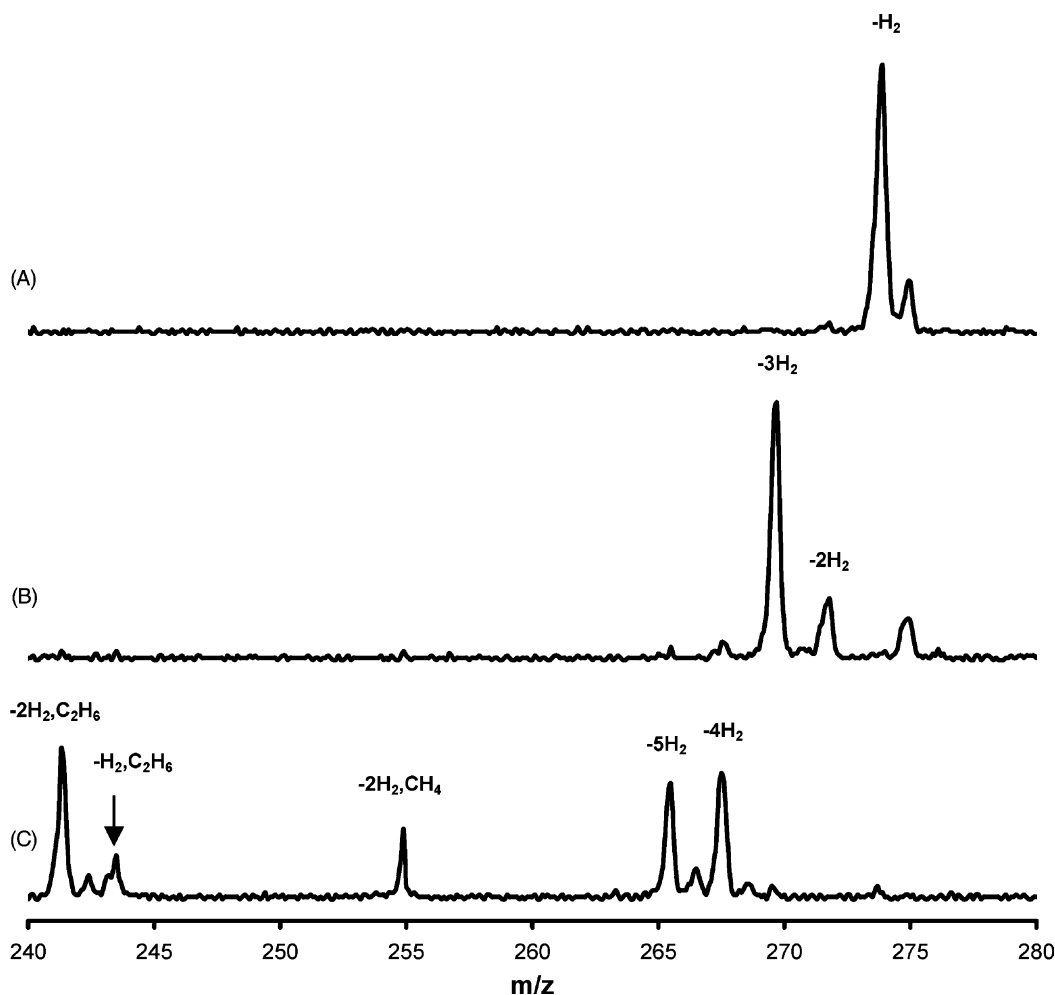


Fig. 1. Mass spectra for collision-induced dissociation of the mass isolated $\text{La}[\text{HCp}^* - \text{H}_2]^+$ product at increasing excitation voltages: (A) $100 \text{ mV}_{\text{p-p}}$; (B) $180 \text{ mV}_{\text{p-p}}$; (C) $600 \text{ mV}_{\text{p-p}}$. The small peak at $m/z = 274$ is assigned as the $\text{La}[\text{C}_9^{12}\text{C}_3^{13}\text{H}_{14}]^+$ isotopologue of the resonantly excited $\text{La}[\text{C}_9^{12}\text{C}_3^{10}\text{H}_{14}]^+$ ion at $m/z = 273$.

3.3.2. Effects of bath gas pressure

It was demonstrated above that CID of a particular product results in further fragmentation via loss of neutral molecules. The Ln^+ ions for both the ICR and QIT experiments were cooled prior to carrying out the reactions, although complete thermalization cannot be assumed in either case. It is not expected that the cooled ICR ions, even if not fully thermalized, would have sufficiently greater energies compared with ions in the QIT to account for the large differences in product distributions. A key difference between the two experimental approaches is the pressure regimes during the reaction periods, $\sim 4 \times 10^{-4}$ Torr bath gas in the QIT vs. $\sim 10^{-7}$ Torr reagent gas in the ICR.

Schröder et al. [48] have examined the effects of pressure on ion–molecule reactions. These authors examined the reactions of FeO^+ with H_2 and CH_4 by three mass spectrometric techniques which operate over a wide range of pressures: ICR at $< 10^{-6}$ Torr; guided ion beam (GIB) at $\sim 10^{-3}$ Torr; and selected ion-flow tube (SIFT) at ~ 1 Torr. Particularly notable was the substantial difference in branching ratios for the reaction with CH_4 . The results of Schröder et al. [48] demonstrated that low-energy pathways were favored in the relatively high-pressure SIFT experiments. The ion–neutral collision frequencies for these three techniques are $< 10^{-3} \text{ ms}^{-1}$ for ICR, $\sim 1 \text{ ms}^{-1}$ for GIB, and $\sim 10^4 \text{ ms}^{-1}$ for SIFT [48]; typical interaction times are $\sim 10 \text{ ms}$ for ICR and SIFT, and $\sim 0.1 \text{ ms}$ for GIB [48]. Accordingly, it can be inferred that during a reaction experiment, following the initial ion thermalization, < 1 collision occurs, on average, for ICR and GIB, whereas on the order of $\sim 10^5$ collisions occur for SIFT. The number of collisions during a QIT experiment is intermediate between these values, depending on the experimental parameters. McLuckey et al. [49] estimated a collision frequency of $\sim 50 \text{ ms}^{-1}$ for a $m/z = 100$ ion in a QIT operating with a He pressure of 10^{-3} Torr. Using the Langevin reaction rate equation, [50] and a value for the polarizability of Ne of $3.956 \times 10^{-25} \text{ cm}^{-3}$ [50], we calculate a collision frequency for $\text{La}[\text{HCp}^*]^+$ of $\sim 5 \text{ ms}^{-1}$ at 4×10^{-4} Torr Ne. At 1×10^{-5} Torr, the lowest Ne pressure for which we obtained QIT prod-

uct distributions, a collision frequency of $\sim 1 \text{ ms}^{-1}$ is estimated by this approach.

In view of demonstrated effects of pressure on product distributions for the $\{\text{FeO}^+ + \text{CH}_4\}$ reaction [48], it was of interest to examine effects of pressure on the QIT product distributions for a reaction of a metal ion with HCp^* to ascertain if the pressure difference between the ICR and QIT experiments might play a role in the consistently discrepant branching ratios. The optimal experimental conditions corresponded to a Ne bath gas pressure of $\sim 4 \times 10^{-4}$ Torr, but it was possible to perform product distribution measurements for pressures in the range of 1×10^{-4} Torr to 1.3×10^{-3} Torr. The results are shown in Fig. 2 as the product distributions as a function of pressure; minor products are not included in Fig. 2 for clarity, but are in accord with the general observations and interpretations. The ICR results of Marçalo et al. [21] are included in Fig. 2 as the disconnected points at 0×10^{-4} Torr (the operating pressure in the ICR experiments of $\sim 10^{-7}$ Torr is essentially zero on the scale of Fig. 2).

Above a bath gas pressure of 3×10^{-4} Torr, the product distributions remain nearly constant and are similar to those obtained at the standard operating pressure of 4×10^{-4} Torr. The data obtained for pressures below 3×10^{-4} Torr reveal a dramatic change in branching ratios, with an increasing degree of fragmentation at lower pressures. At high pressures, H_2 - and CH_4 -elimination are dominant whereas at low pressures the elimination of 2H_2 and 3H_2 (as well as $\{\text{H}_2, \text{CH}_4\}$ and $\{2\text{H}_2, \text{CH}_4\}$, which are not included in Fig. 2) become increasingly important reaction channels. It is apparent from the results in Fig. 2 that the QIT branching ratios obtained at relatively low pressures move toward those for the very low-pressure ICR experiments. It is likely that different populations of excited state metal ions, M^{*+} , are produced in the QIT glow discharge and the ICR laser desorption ion sources. Although M^{*+} chemistry could account for some of the greater extent of fragmentation under the ICR conditions, that no high-energy fragmentation channels (i.e. insertion products) were observed for Sm^{*+} suggests that this effect is insignificant under

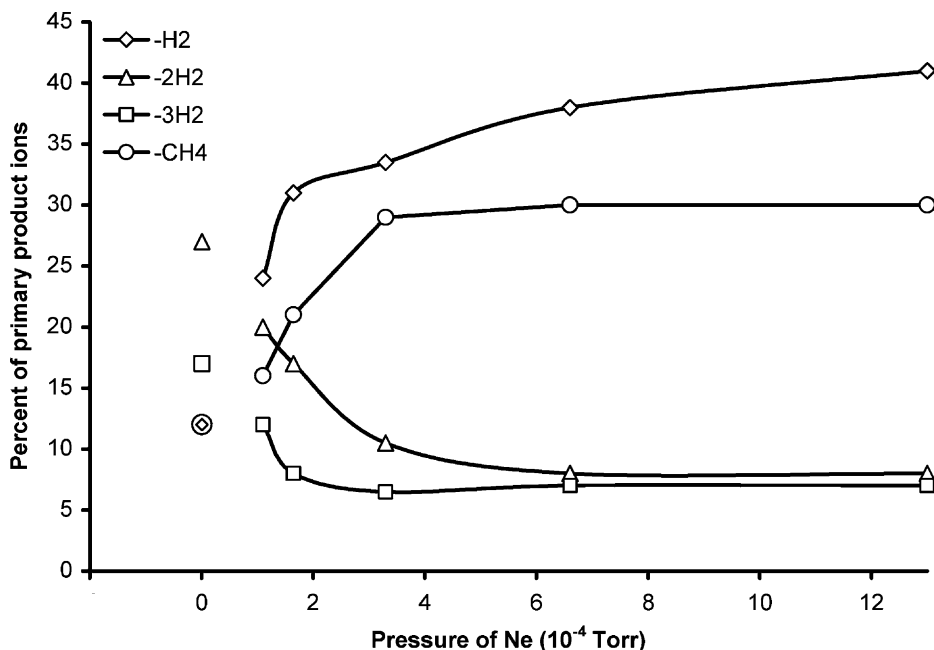


Fig. 2. Primary product distribution for the $\{\text{La}^+ + \text{HCp}^*\}$ reaction as a function of increasing neon pressure in the ion trap. All experiments were carried out using a HCp^* pressure of $\sim 5 \times 10^{-7}$ Torr and a reaction time of ~ 10 ms. The low-pressure ICR results from Marçalo et al. [21] are included at near zero pressure on this scale. The product ions correspond to $\text{La}[\text{HCp}^* - E]^+$, where the aggregate eliminated E are indicated.

both the ICR and QIT conditions. Furthermore, because collisional de-excitation of M^{*+} is generally inefficient, the substantial changes in branching ratios upon varying the QIT bath gas pressure is not likely attributable to changes in the amount of M^{*+} available for reaction. To substantiate this interpretation, reaction times in the QIT were varied between 10 and 60 ms, with a concomitant increase in the product yields for longer reaction times. If collisional de-excitation of M^{*+} were a significant factor, changes in branching ratios should have occurred as the reaction time was varied. Specifically, a lesser degree of fragmentation for longer reaction times would be expected due to more efficient de-excitation of some of the metal ions that reacted towards the end of the reaction period if collisional de-excitation of M^{*+} was occurring. No significant change in branching ratios was found as reaction times were varied, confirming that M^{*+} chemistry could not reasonably account for the bath gas pressure effect on the QIT results.

We conclude that the differences in product distributions between the ICR and QIT experiments can be attributed to the different pressure regimes of the two techniques, and that QIT results approach those obtained by ICR when low bath gas pressures are employed. The primary product ions, such as $\text{Ln}[\text{HCp}^* - \text{H}_2]^+$, are produced in exothermic reactions, with the heat of reaction deposited in the complex. In the absence of rapid radiative decay or third-body collisional cooling of some of the nascent hot products, subsequent elimination processes can proceed, which may be adiabatically endothermic and therefore, would not be seen under thermoneutral conditions. In analogy with the postulated quenching of reactive intermediates under high-pressure SIFT conditions [48], we propose that under the typical QIT operating conditions of 4×10^{-4} Torr Ne (~ 5 collisions ms^{-1}) the nascent products are collisionally cooled by the bath gas prior to extensive sequential fragmentation after the initial exothermic process(es).

When the pressure is reduced to 1×10^{-4} Torr Ne, (~ 1 collision ms^{-1}), the (four-fold) decrease in collision frequency evidently results in a significantly greater degree of fragmentation before collisional cooling can occur. The low-pressure QIT results in Fig. 2 can be extrapolated to give the ICR product distributions that were obtained at collision frequencies of $< 1 \text{ ms}^{-1}$.

The discrepant product branching ratios for the LnO^+ reactions between ICR and QIT (Table 4) can similarly be attributed to the different pressure regimes. If the initial association complex, structure 1 in Schemes 1 and 2 ($\text{M}^+ = \text{LnO}^+$), then the energy associated with adduct formation can be dissipated through low-energy collisions with the bath gas. It may be that some dehydration processes become endothermic absent the energy provided by the initial $\text{LnO}^+ \cdot \text{HCp}^*$ interaction energy. Although all of the net reactions observed by both QIT and ICR are considered to be either nearly thermoneutral or exothermic, extraction of energy from the two-body reaction system at intermediate steps by collisional cooling can evidently render certain processes energetically inaccessible.

The ability to determine the product distributions at even lower pressures in the QIT was restricted by Ne gas originating from the high-pressure glow-discharge ion source, and limited pumping speed in the differentially pumped ion trap region. It should be possible to study this effect at even lower pressures in a modified QIT, for example by using a laser desorption ionization rather than a high-pressure glow discharge ion source. The product distributions were found to be similar using He, Ne and Ar as a bath gas at 4×10^{-4} Torr, but it would be of interest to study the quenching effect as a function of pressure for different bath gases. The HCp^* substrate appears to be particularly susceptible to the pressure effect, due to its intrinsically fragile nature towards exothermic decomposition [21] and the wide variety of available sequential reaction channels. The results of Schröder et al. [48] demonstrated the effects of pressure on branching ratios by comparison of the same reaction using different mass spectrometric techniques that operate in very different pressure regimes. The present experiments have demonstrated

similar results employing a single instrument operating over a relatively narrow range of pressures.

It is somewhat fortuitous that the pressures accessible in these QIT experiments extended into a range where pressure effects on the branching ratios for the $\{\text{La}^+ + \text{HCp}^*\}$ reaction became clearly evident. The results in Fig. 2 suggest that at the higher pressures, the bath gas in the ion trap is acting as a chemically inert gas-phase “solvent” which serves to mediate high-energy processes. In this regard, it is possible to study reactions under a range of conditions which link the single-collision environment of the ICR, and other low-pressure mass spectrometric techniques, with those of multiple-collision environments. This represents a step towards better understanding the relationship between isolated gas-phase ion–molecule reactions, and chemistry that occurs in the condensed phase.

4. Conclusions

The utility of the QIT for studying reactions between bare and oxo-ligated metal ions and an organic molecule has been demonstrated with this work. Reactions of metal and metal oxide ions with HCp^* were studied, with an emphasis on two actinides, thorium and uranium, as well as representative lanthanides. The reaction branching ratios, as reflected in the product distributions, were qualitatively similar to those previously found for the lanthanides by ICR [21]. For the Ln^+ , two distinctive types of reactivity were evident that reflect the electronic structure and energetics at the metal center. The distinctive product distributions for Th^+ are interpreted in the context of thorium as a quasi-d-block group IV transition metal ion with three chemically active valence electrons. The chemistry of U^+ with HCp^* was generally similar to those Ln^+ which react via an insertion type of mechanism; discrepancies may reflect the greater chemical activity of the quasi-valence 5f electrons of uranium compared with the 4f electrons of the lanthanides.

The secondary product distributions for the Ln^+ were also qualitatively consistent with those from

ICR experiments [21]. The results for Th^+ indicate addition of an HCp^* molecule as the main secondary reaction. This contrasts with the elimination of additional H_2 molecules in the case of Ta^+ , which is a highly reactive transition metal ion—although Th^+ exhibits d-block behavior, it is not as reactive towards HCp^* as Ta^+ . The secondary reactions for U^+ were particularly intriguing and motivated examination of reactions of isolated precursors. It was found that two of the primary products, $\text{U}[\text{HCp}^* - \{3\text{H}_2\}]^+$ and $\text{U}[\text{HCp}^* - \{2\text{H}_2, \text{CH}_4\}]^+$, exhibited reactivity towards a second HCp^* which indicates two covalent organouranium bonds in the primary complexes. Such uranium–carbon covalent bonding is well established in condensed phase organometallic chemistry, as discussed by Marks [51]. It would appear probable that one of the organouranium complexes incorporates carbene-type bonding.

As with the bare ions, the QIT results for the studied LnO^+ were qualitatively consistent with those from ICR for both the primary and secondary product distributions. In distinct contrast to the relatively inert LnO^+ , both ThO^+ and UO^+ exhibited reaction product distributions remarkably similar to those of bare Sm^+ . We conclude that one chemically active valence electron is needed at the metal center for the non-insertion activation of HCp^* to proceed efficiently. For ThO^+ , this is likely a non-5f electron, in accord with the generally d-block character of thorium. However, the 5f electrons of uranium are substantially lower in energy and more spatially localized. The results for UO^+ suggest an active role of uranium 5f electron(s) in its gas-phase reactions with HCp^* , either via their direct participation in bonding, as postulated by Cornehl et al. [9], or perhaps rather through promotion/hybridization with the outer valence 6d/7s orbitals.

Although the present QIT results were qualitatively similar to the previous ICR results for lanthanide ions [21], significant differences were apparent in the product distributions. Specifically, a greater degree of fragmentation occurred in the ICR. The CID results in the QIT demonstrated that “heating” of the

$\text{La}[\text{HCp}^* - \text{H}_2]^+$ product resulted in fragmentation reminiscent of that in the ICR. Because the QIT experiments were performed at much higher pressures than the ICR experiments, the branching ratios for the $\{\text{La}^+ + \text{HCp}^*\}$ reaction were examined as a function of pressure. It was found that the product distributions in QIT approached those in the ICR as the QIT bath gas pressure was decreased. We interpret this to indicate that the QIT bath gas can be considered as an inert gas-phase “solvent” that serves to collisionally cool hot nascent products, and thereby suppress high-energy fragmentation channels.

The QIT has been demonstrated as a suitable approach for investigating gas-phase organometallic chemistry via reactions between metal ions and a reactant gas. The present study focused on reaction branching ratios for efficient reactions with HCp^* , but this technique is also well-suited to measuring reaction rates. A particular advantage of the QIT compared with alternative techniques is its compact size. This attribute will be particularly advantageous for studying the chemistry of highly radioactive and short-lived actinides in a glovebox. The QIT approach is quite versatile and can be operated under diverse experimental conditions and using a variety of ion sources, both external (as in the present study) and internal to the trap. The CID and bath gas results of the present study are illustrative of the flexibility of the QIT, and the bath gas effect is particularly intriguing as a relatively facile means to probe relationships between condensed and gas-phase organometallic chemistry.

Acknowledgements

Research sponsored by the Division of Chemical Sciences, Geosciences and Biosciences, Office of Basic Energy Sciences, U.S. Department of Energy under contract DE-AC05-00OR22725 with Oak Ridge National Laboratory, managed and operated by UT-Battelle, LLC. The authors would like to thank Dr. Joaquim Marçalo of Instituto Tecnológico e Nuclear for helpful comments.

References

- [1] K. Eller, H. Schwarz, *Chem. Rev.* 91 (1991) 1121.
- [2] B.S. Freiser (Ed.), *Organometallic Ion Chemistry*, Kluwer, Dordrecht, 1996.
- [3] Y. Huang, M.B. Wise, D.B. Jacobson, B.S. Freiser, *Organometallics* 6 (1987) 346.
- [4] Y.A. Ranasinghe, T.J. MacMahon, B.S. Freiser, *J. Am. Chem. Soc.* 114 (1992) 9112.
- [5] W.W. Yin, A.G. Marshall, J. Marçalo, A. Pires de Matos, *J. Am. Chem. Soc.* 116 (1994) 8666.
- [6] C. Heinemann, D. Schröder, H. Schwarz, *Chem. Ber.* 127 (1994) 1807.
- [7] H.H. Cornehl, C. Heinemann, D. Schröder, H. Schwarz, *Organometallics* 14 (1995) 992.
- [8] H.H. Cornehl, R. Wesendrup, J.N. Harvey, H. Schwarz, *J. Chem. Soc., Perkin Trans. 2* (1997) 2283.
- [9] H.H. Cornehl, R. Wesendrup, M. Diefenbach, H. Schwarz, *Chem. Eur. J.* (1997) 1083.
- [10] J.M. Carretas, A. Pires de Matos, J. Marçalo, M. Pissavini, M. Decouzon, S. Gèribaldi, *J. Am. Soc. Mass Spectrom.* 9 (1998) 1035.
- [11] N. Marchandé, S. Breton, S. Gèribaldi, J.M. Carretas, A. Pires de Matos, J. Marçalo, *Int. J. Mass Spectrom.* 195/196 (2000) 139.
- [12] J. Marçalo, J.P. Leal, A. Pires de Matos, *Int. J. Mass Spectrom. Ion Processes* 157/158 (1996) 265.
- [13] J. Marçalo, J.P. Leal, A. Pires de Matos, A.G. Marshall, *Organometallics* 16 (1997) 4581.
- [14] Z. Liang, A.G. Marshall, A. Pires de Matos, J.-C. Spirlet, in: L.R. Morss, J. Fuger, (Eds.), *Tranuranium Elements—A Half Century*, American Chemical Society, Washington, DC, 1992, p. 247.
- [15] C. Heinemann, H.H. Cornehl, H. Schwarz, *J. Organomet. Chem.* 501 (1995) 201.
- [16] D.C. Duckworth, J.R. Eyler, C.H. Watson, in: C.M. Barshick, D.C. Duckworth, D.H. Smith (Eds.), *Inorganic Mass Spectrometry: Fundamentals and Applications*, Marcel Dekker, New York, 2000, p. 329.
- [17] R.F. Bonner, G. Lawson, J.F. Todd, *Int. J. Mass Spectrom. Ion Phys.* 10 (1972/73) 197.
- [18] J. Shen, J.S. Brodbelt, *Int. J. Mass Spectrom.* 176 (1998) 39.
- [19] C. Hao, R.E. March, *Int. J. Mass Spectrom.* 212 (2001) 337.
- [20] J. Marçalo, A. Pires de Matos, W.J. Evans, *Organometallics* 15 (1996) 345.
- [21] J. Marçalo, A. Pires de Matos, W.J. Evans, *Organometallics* 16 (1997) 3845.
- [22] J.K. Gibson, *Int. J. Mass Spectrom.* 202 (2000) 19.
- [23] F.L. King, W.W. Harrison, *Int. J. Mass Spectrom. Ion Processes* 89 (1989) 171.
- [24] D.C. Duckworth, R.K. Marcus, *J. Anal. Atom. Spectrom.* 7 (1992) 711.
- [25] S.A. McLuckey, G.L. Glish, D.C. Duckworth, R.K. Marcus, *Anal. Chem.* 64 (1992) 1606.
- [26] D.E. Goeringer, K.G. Asano, S.A. McLuckey, D. Hoekman, S.W. Stiller, *Anal. Chem.* 66 (1994) 313.
- [27] K.J. Hart, S.A. McLuckey, *J. Am. Soc. Mass Spectrom.* 5 (1993) 250.
- [28] A. Colorado, J. Brodbelt, *J. Am. Soc. Mass Spectrom.* 7 (1996) 1116.
- [29] G.P. Jackson, F.L. King, D.E. Goeringer, D.C. Duckworth, *Int. J. Mass Spectrom.* 216 (2002) 85.
- [30] J.N. Louris, R.G. Cooks, J.E.P. Syka, P.E. Kelly, G.C. Stafford, J.F.J. Todd, *Anal. Chem.* 59 (1987) 1677.
- [31] F. Nakao, *Vacuum* 25 (1975) 431.
- [32] J.E. Bartmess, R.M. Georgiadis, *Vacuum* 33 (1983) 149.
- [33] J. Blaise, J.-F. Wyart, *Energy Levels and Atomic Spectra of Actinides*, Tables Internationales de Constantes, Paris, 1992.
- [34] W.C. Martin, R. Zalubas, L. Hagan, *Atomic Energy Levels—The Rare Earth Elements*, U.S. Department of Commerce, Washington, DC, 1978.
- [35] C.E. Moore, *Atomic Energy Levels*, Vol. III, U.S. Department of Commerce, Washington, DC, 1958.
- [36] D.L. Hildenbrand, L.V. Gurvich, V.S. Yungman, *The Chemical Thermodynamics of Actinide Elements and Compounds. Part 13: The Gaseous Actinide Ions*, International Atomic Energy Agency, Vienna, 1985.
- [37] M.S. Chandrasekharaiiah, K.A. Gingerich, in: K.A. Gschneidner, Jr., L. Eyring (Eds.), *Handbook on the Physics and Chemistry of Rare Earths*, Vol. 12, Elsevier, Amsterdam, 1989, p. 409.
- [38] S.G. Lias, J.E. Bartmess, J.F. Liebman, J.L. Holmes, R.D. Levin, W.G. Mallard, *Gas-Phase Ion and Neutral Thermochemistry*, American Chemical Society, Washington, DC, 1988.
- [39] E.G. Rauh, R.J. Ackermann, *J. Chem. Phys.* 60 (1974) 1396.
- [40] R.J. Ackermann, E.G. Rauh, R.J. Thorn, *J. Chem. Phys.* 65 (1976) 1027.
- [41] W.G. Mallard (Ed.), *NIST Chemistry WebBook*. NIST Standard Reference Database Number 69—July 2001 Release, National Institute of Standards and Technology: Gaithersburg, MD, 2001 (<http://webbook.nist.gov/chemistry/>).
- [42] D. Schröder, H. Schwarz, S. Shaik, in: B. Meunier (Ed.), *Metal-Oxo and Metal-Peroxo Species in Catalytic Oxidations*, Springer, Berlin, 2000, p. 91.
- [43] T.J. Marks, A. Streitwieser, Jr., in: J.J. Katz, G.T. Seaborg, L.R. Morss (Eds.), *The Chemistry of the Actinide Elements*, 2nd Edition, Vol. 2, Chapman & Hall, London, 1986, p. 1547.
- [44] Y. Huang, B.S. Freiser, *J. Am. Chem. Soc.* 112 (1990) 5085.
- [45] K.J. Hart, S.A. McLuckey, *J. Am. Soc. Mass Spectrom.* 5 (1994) 250.
- [46] S.A. McLuckey, D.E. Goeringer, *J. Mass Spectrom.* 32 (1997) 461.
- [47] R.C. Dunbar, *Int. J. Mass Spectrom.* 200 (2000) 571.
- [48] D. Schröder, H. Schwarz, D.E. Clemmer, Y. Chen, P.B. Armentrout, V.I. Baranov, D.K. Böhme, *Int. J. Mass Spectrom. Ion Processes* 161 (1997) 175.
- [49] S.A. McLuckey, G.L. Glish, K. Asano, J.E. Bartmess, *Int. J. Mass Spectrom. Ion Processes* 10 (1991) 171.
- [50] D.R. Lide (Ed.), *CRC Handbook of Chemistry and Physics*, 81st Edition, CRC Press, New York, 2000, p. 10.
- [51] T.J. Marks, in: J.J. Katz, G.T. Seaborg, L.R. Morss (Eds.), *The Chemistry of the Actinide Elements*, 2nd Edition, Vol. 2, Chapman & Hall, London, 1986, p. 1588.